

Reviewer 1

We would like to acknowledge the insightful comments and suggestions provided by reviewer 1. We will consider the reviewer's suggestions in our revised manuscript.

Followings are the responses (R) based on the comments:

(1) The description of the GC approach appears to be somewhat ambiguous: While Sect. 2 is claiming to use L1B KBRR data only, it becomes clear from Sect. 3 that in fact L2 monthly normal equations from ITSG2016 are applied. Those NEQ, however, include not only KBRR but all GRACE sensor information (KBRR, ACC, GPS, attitude) and a priori background models (AOD1B, earth, ocean, and atmospheric tides, third body effects).

R1: Reviewer is correct that the normal equation is built including measurements from all GRACE sensors, including KBR, and a priori background models. Therefore, lines 144 – 145 of the revised manuscript is revised as follows:

“... the observation vector containing various kinds of L1B data including the inter-satellite ranging”

I suggest that comparisons with the official ITSG2016 monthly solutions are included in order to demonstrate the added-value of the GC approach over the standard L2 data. Note that comparisons against GRGS or JPL monthly solutions as already (partly) included in the paper will not be sufficient since ITSG2016 is commonly perceived as a GRACE series of particularly high quality.

R2: The computation of ΔTWS from ITSG L2 solutions (like other L2 solutions) is subject to the post-processing filters and often followed by the application of empirical scaling factors, obtained from the land surface models. Our study provides a more rigorous way of computing ΔTWS without going through such ad hoc procedures. GRGS and JPL mascon are internally or post-processed and it is not expected users to apply (subjective) post-processing. This is the primary reason we validate our results with GRGS and JPL mascon.

(2) The GC approach assumes that model errors are normally distributed with zero mean (eq. 1). Authors should provide more evidence that this assumption is indeed justified in their setting.

R3: As the reviewer concerned, the GC approach is developed based on the least-square combination, which assumes the uncertainty following the normal distribution with zero mean and covariance C. The derivation and setting of model uncertainty under the given assumption (e.g., zero mean) and its limitation are clarified in Sect. 4.2. For clarity, we modify lines 298 – 301 of the revised manuscript as follows:

“The GC approach assumes that model errors are normally distributed with zero mean. Any violation of this assumption will yield a bias in the combined solutions. Therefore, the mean value is removed from each ensemble member, $\mathcal{H}_R' = \mathcal{H}_R - \tilde{h}_R$, and the error covariance matrix of the model is empirically computed as”

(3) line 284: It is optimistic to assume that the model omission error can be fully accounted by just increasing the model covariance by 20%, in particular since this assumes that omission errors do not contribute to biases (which is quite unlikely). More evidence need to be provided for the (approximate) validity of this assumption.

R4: Rigorous development of the statistical property of the land surface models (expectation and covariance) is crucial but a difficult task. The empirical way was taken in this study. As also noted by the reviewer, the omission will likely introduce a bias in the solutions as well.

We acknowledge this in the last paragraph of Section 4.2. Lines **313 – 319** of the revised manuscript now reads:

“It is emphasized that the model omission error caused by imperfect modelling of hydrological process within the LSM is not taken into account in the above description. The omission error may increase the model covariance and introduce a bias as well. We account for the omission error by increasing 20% of the model covariance. (i.e., multiplying C_R by 1.2). We determine such omission error based on trial-and-error such that it increases the model error (due to the omission error) but not exceeds the model error value reported by Dumedah and Walker (2014). We acknowledge that this is only a simple practical way of accounting for the omission error into the total model error.”

(4) The statement of line 212ff is unclear (and apparently not picked up again in the remainder of the paper). Please elaborate.

R5: This is to introduce what other independent GRACE solutions (GRGS and JPL mascon) to be used to compare our GC results. The solutions are used in Sect. 5.2 and 5.5 in the revised manuscript.

(5) Line 289: What does "cooperating" mean in that case?

R6: Replaced with “using” in the revised manuscript.

(6) The specific yield for the Queensland and Victoria networks differ by a factor of 2: Is there any geologic evidence/argument available for those very different yield factors?

R7: We took the specific yield values simply from the literatures (Chen et al., 2016; Rassam et al., 2013, Welsh 2008).

(7) Sect. 6.2 appears to be rather an outlook to a future study. Since no actual results are presented, I am wondering if this section should not be better removed entirely?

R8: We thank for reviewer’s suggestion. Section 6.2 is removed from the manuscript.as suggested.

(8) Major mining activities are currently taking place at the North West Plateau where GRACE picks up negative mass trends: What measures have been taken to reduce mass loss un-related to the terrestrial water cycle from the GRACE data in particular in that area?

R9: Reviewer made a good point. However, it is likely that the negative mass trends is mainly caused by the declining rainfall after 2000 (van Dijk et al., 2011), and less likely mining activity, as confirmed by the government WA Department of Water.

<http://www.news.com.au/technology/environment/climate-change/nasa-study-says-the-canning-basin-in-wa-is-being-depleted-too-fast/news-story/9bf107b8299c19b57904ed719639a0ba>

Reference

van Dijk, A. I. J. M., L. J. Renzullo, and M. Rodell (2011), Use of Gravity Recovery and Climate Experiment terrestrial water storage retrievals to evaluate model estimates by the Australian water resources assessment system, *Water Resour. Res.*, 47, W11524, doi:10.1029/2011WR010714.

Reviewer 2

We would like to acknowledge the insightful comments and suggestions provided by reviewer 2. We will consider the reviewer's suggestions in our revised manuscript. Followings are the responses (R) based on the comments:

Line 152: Equation 9 is the most important equation in this study, but some of the information is provided in the later section 3. Also the model covariance matrix is provided in section 4.2. Authors might consider making the method section clearer and reduce some unnecessary equations.

R1: We organize the paper to introduce mathematical developments and followed by implementation. Section 2 describes the general methodology, while sections 3 and 4 describe the specifics needed to implement the algorithm with the ITSG data and CABLE model, respectively. We believe this is a logical presentation of our methods. This is clarified in the revised manuscript, lines 116 – 120 as follows:

“Firstly, the derivation of GC approach is presented in Sect. 2 while the description of GRACE data processing, including the use of GRACE normal equation is given in Sect. 3. Secondly, the CABLE modelling is outlined in Sect. 4. This includes the derivation of model uncertainty based on the quality of precipitation data and the model parameter inputs.”

Line 170: Basically, the paper claimed “the use of intersatellite tracking data”, but the data was the normal matrix N and vector c obtained from the ITSG-Grace 2016 as well as the gravity field coefficient from GOCO05s solution. No Level 1B data was actually used directly in this study, so I wonder whether the title is appropriate.

R2: As reviewer pointed out correctly, we started from the L1B normal equation data, not directly from L1B data. We revised the titles as follows: “On the use of GRACE normal equation of intersatellite tracking data for improved estimation of soil moisture and groundwater in Australia”.

Line 195: The GRGS gridded TWS products were used in Equation 9 to work out the TWS values outside Australia. The L3 GRGS products derived from the Earth’s geopotential coefficients up to degree and order 80, while ITSG data used in the study were up to 90. Why not using the ITSG TWS data? Can the ITSG normal equation represent the uncertainty in L3 GRGS products?

R3: Eq. (9) requires the knowledge of ΔTWS grid outside the study region. However, the ITSG does not provide such gridded data directly. GRGS solution is one of the best possible candidate suitable for correcting the outside effect since it is most compatible with normal equation dataset we use in terms of a resolution and it does not require the (subjective) post-processing of the solutions unlike ITSG and other L2 solutions. This is clarified in lines 240 – 241 of the revised manuscript.

Line 210: The gridded GRGS data was resampled to 0.5 degree spatially, but the normal equation only contains the information to degree 90. How did you deal with the different spatial scale in the error variance-covariance matrix?

R4: This study uses the least-square combination approach in spatial domain. It is possible to compute the ΔTWS from the normal equation at any spatial scale (here is 0.5 degree). However, it is noted that the 0.5 degree data are spatial correlated (because of 90 degree resolution), and such correlation in the 0.5 degree grid is already accounted in the GC approach described in Sect. 2.

Line 231: depth between 0.022 m not cm

R5: Reviewer is correct. We correct 0.022 cm to 0.022 m in the revised manuscript.

Line 256: The sensitivity study of the model parameters is an important process but not necessary to show in the paper. Author may consider removing table 2.

R6: We thank for reviewer’s suggestion. We still believe that Table 2 is worth to present since it gives an insight about the model parameters in a direct relevance to the storage outputs. Therefore, we decide to keep Table 2 in the revised manuscript.

Line 298: Did you do the CDF matching for few years and validate the results for the rest of time period? Or did you match all the time series and validate the same time period? If so, your estimates and observations are not independent. The CDF matching may discard important signals of the observations. Since only correlation was calculated, CDF matching is not necessary.

R7: We built the CDF using 2003-2004 data and applied it to the rest. As the NS coefficient (not correlation coefficient) is used in this section, the remaining bias might result in poor NS values, the bias correction is then necessary. For clarity, we added the additional statement in lines [335 – 336](#) of the revised manuscript as follows:

“The CDF is built using the 2003-2004 data, and it is used for the entire period”

Line 301: The variability of soil moisture inside a basin is quite high. The average of basin and monthly soil moisture can smooth out lot of signals. Since your output is 0.5_x 0.5_ gridded products, why not validate at this scale instead of basin scale? Can you show some validation with in-situ measurements?

R8: We indeed conducted the analysis at 0.5x0.5 scale (for surface SM), and it provides very similar conclusions to the basin mean. Both results do not show the significant improvement for the surface soil moisture computation, which is supported by the recent publication (Tian, et al., 2017). We discussed why this is the case and the limitation of GRACE data in the original manuscript.

Line 307: The groundwater estimates were only validated for two states using the state average. It should be possible to validate all the states over Australia or at basin scale to be consistent with other results. Two states are not sufficient to support the improvement in groundwater storage estimates over Australia.

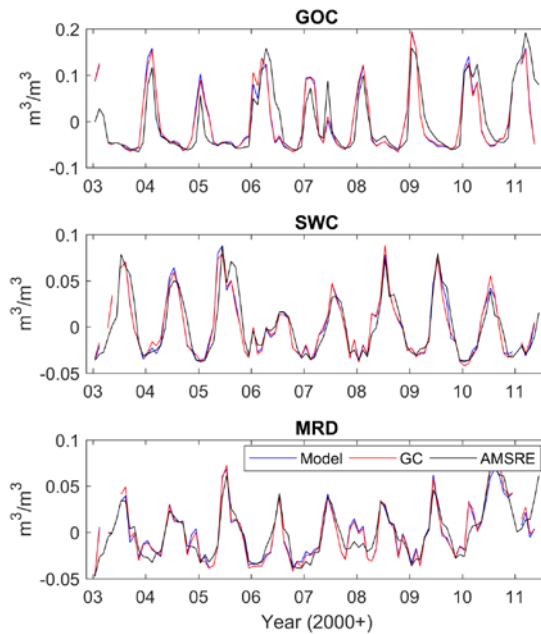
R9: We agree with reviewer. However, the primary purpose is to demonstrate a statistically rigorous way of using GRACE datasets (not high level processed data) for combining with the LSM models and eventually for data assimilation by emphasizing the importance of using error propagation and full covariance. The ground observation network of Australia is relatively sparse particularly at the state-wide level. Our study is initially based on what we could get.

Line 320: Is that only one value of specific yield per state was used to convert the groundwater level to storage? Will it be more appropriate to use different specific yields for different locations and calculate the average?

R10: We agree with reviewer that it is ideal to conduct the conversion at all grid cell independently. However, no such information is available at the grid cell level. We used the best possible knowledge of specific yield from the published literatures.

Line 468: The difference between model and GC approach for soil moisture is marginal here for basin monthly average. Can you show some time series examples of GC results and AMSR-E retrievals?

R11: Below are the examples of the time series between our estimates and AMSR-E (C-band):



The statistical value can be found in **Table 3** of the revised manuscript. As stated in the manuscript, no significant change is seen in GC solution, likely due to limitation of GRACE’s temporal and spatial resolution. This same conclusion was reported by Tian et al. (2017). We provide a reference and recommendation how SM estimates can be improved in the conclusion section, lines **704 – 710** of the revised manuscript.

“it is challenging to improve surface soil moisture varying rapidly in time, using a monthly mean GRACE observation. Tian et al. (2017) utilized the satellite soil moisture observation from the Soil Moisture and Ocean Salinity (SMOS, Kerr et al., 2001) in addition to GRACE data for their data assimilation and showed a clear improvement in the top soil moisture estimate. The GC approach with complementary observations at higher temporal resolution should be considered particularly to enhance the surface soil moisture computation.”

Line 482: In Table 4, the trend of GC approach is about one third of in-situ measurements for Queensland. What causes such big difference?

R12: As a matter of fact that the GC approach optimally combines the GRACE observation with the model results, the GC result is inevitably influenced by the model estimate. As seen in Fig. 7 and 9, the GC result moves toward the in situ measurement but it is still influenced by the Δ GWS estimation from the model.

Line 491: It will be interesting to see the groundwater storage change in Murray-Darling Basin after the GC approach compared with in-situ measurements, during the big drought and big wet period.

R13: The reviewer’s suggestion is very interesting. However, we did not have the in situ groundwater data of the Murray-Darling Basin by the time of this study and so we conducted the analysis based on what we could obtain. We will consider the validation in the Murray-Darling Basin in our future study.

Line 502: This section investigates the mass variation in the past 13 years based on the GC approach. Figure 8 is a quite good demonstration of the mass variation at different layers of water storage. The top and root-zone soil moisture show quite different trends. The root-zone soil moisture has similar trends with TWS and groundwater for most of the basins. It will be better to have some validation of root-zone soil moisture estimates and more sufficient groundwater storage estimates to support the analysis in this section.

R14: We appreciate reviewer suggestion and we strongly agree. However, similar to what we stated above, we did not have an access to the in situ root-zone soil moisture of Australia, and the validation

of such a component was not possible. We would like to reiterate that this is the first demonstration of new technique of using more fundamental dataset from GRACE, applied to the Australian continent.

Line 579: 0.39 is App1 and 0.42 is App2? So the trend calculating from GRACE subtracting modeled soil moisture is the same with modeled groundwater trend (in Table 4). The NS value for App1 is 0.46, which is less than the CABLE model without GRACE? For Victoria, the NS value of App2 is 0.3 less than CABLE model without GRACE too. With the assimilation of GRACE in App2, the correlation is degraded. It seems model itself without GRACE is better compared to App1 or App2. Still, for only two states validation results, it's hard to demonstrate that GC approach works better due to the error information. It could be your model uncertainty is better estimated using the ensembles as explained in Section 4.2. When you do the App1 and App2, did you also used 7 precipitation dataset as the same as the GC approach? Please clarify.

R15: Reviewer is correct that App1 and App2 provide poorer results compared to CABLE (in some case) or GC approach. However, this section demonstrates the scenario when different Δ GWS computation approach are used (not GC). The model part remains the same (as in GC approach). App1 uses mascon solution with error free scenario while App2 uses mascon with its variance matrix, and the different outputs are mainly attributed to the different application of the uncertainty type. The poor results of App1 and App2 are mainly due to too simplified error information implemented. This has been clarified in the revised manuscript lines [630 – 632](#):

“Note that the model uncertainty remains the same as in GC approach (Sect. 4.2). The different outputs between App1 and App2 are mainly attributed to the different application of the different estimates of the uncertainty.”

Line 587: The future work in this section is interesting but no results were provided. Author may consider removing this section completely or providing the results in this paper together with the GC approach.

R16: We thank for reviewer's suggestion. Section 6.2 is removed from the manuscript.as suggested.

Reviewer 3

We would like to thank reviewer 3. Followings are the responses (R) based on the comments:

L15-L16→ This is not true that "there is no covariance matrix for L2 products". After filtering and conversion to TWS, this error can be propagated, which is addressed e.g., in DOI:10.1007/s10712-014-9309-8. L48 repeats the same claim!

R1: Review is correct that the covariance matrix is available for L2 product. However, it is not the case for the gridded product (Level 3) discussed here. This is clearly written in lines **13 – 16** of the submitted manuscript:

"... from the high level products (e.g., land grid). The gridded data products are subjected to several drawbacks such as signal attenuation and/or distortion caused by ad hoc posteriori filters, and a lack of error covariance information."

For clarity, we include the additional information in line **16** of the revised manuscript as follows:

"... from the high level products (e.g., land grid from the Level 3 product). The gridded data products ..."

L16-L17: The consequence is undesired alteration of ... data and its statistical property. It is not clear what this means. Are you suggesting that all other published papers are wrong!?

R2: The post-processed (high level grid) data are often used without a proper statistical information. It changes information GRACE data provides. For clarity, we revised the statement as follows:

"The post-processing process of GRACE data might lead to the undesired alteration of the signal and its statistical property."

L21-L22→ This is not clear which approach has been used.

R3: The approach used in this study is the least-squares combination. This is clearly mentioned in the earlier sentence (lines **19 – 22** of the submitted manuscript):

"The approach combines the GRACE's least-squares normal equation (full error variance-covariance information) of L1B data with the results from the Community Atmosphere Land Exchange (CABLE) model to improve soil moisture and groundwater estimates."

L61-L64→ Inversion techniques for signal separation have been applied, which consider errors in GRACE and complementary data used for signal separation. DOI:10.1016/j.jog.2012.03.001; DOI:10.1016/j.jog.2011.02.003; DOI:10.1007/s10712-016-9403-1

R4: Based on the suggested literatures, the text was revised as follows.

"Several techniques have been developed to separate different signals considering the errors in GRACE and other data (Rietbroek et al., 2012; Schmeer et al., 2012; Forootan et al., 2017). However, the GRACE uncertainty is often derived empirically, not necessarily reflecting the actual GRACE error characteristics. The empirical GRACE errors have been also used in the data assimilation (e.g., Zaitchik et al., 2008; Tangdamrongsub et al., 2015; Tian et al., 2017)."

The Methodology section needs to be specified, please add appendices to clearly how the equations are built. I cannot figure out how the normal equation is formulated, whether it includes KBRR and any orbital information? L120→ Please describe how the matrix A is derived and what are the entries. Similarly L128-L130 are unclear.

R5: As written in the original manuscript, we use the normal equation data from the ITSG-2016. The description of the data can be found in the data webpage provided in the manuscript

(<https://www.tugraz.at/institute/ifg/downloads/gravity-field-models/itsg-grace2016>). As the derivation of the normal equation is not the focus of this study, we do not discuss it further but refer to the description in the data webpage and references therein (this is stated clearly in **Sect. 3.1** of the original manuscript). The element of the matrix A is mainly the partial derivative of the variational equation respect to the orbital information and gravitational coefficients. The variational equation include both orbital information and various kinds of LIB data including KBR data.

The accuracy of recovery has not been justified, which is essential for any scientific application to show that the accuracy of software is comparable with official products. Please include comparisons with the official ITSG2016 monthly solutions.

R6: The objective of this study is to combine GRACE normal equation with land surface model result to improve the estimated SM and GWS, and do not independently resolve the GRACE solution. We already presented the validation of SM and GWS computations. This is stated clearly in the introduction lines **80 – 82** of the submitted manuscript:

“The approach optimally combines the GRACE’s least-squares normal equations with CABLE to improve ΔSM and ΔGWS estimates.”

Therefore, the accuracy of the estimated result is only compared with the model-only result (please see **Fig. 6**). The accuracy of our TWS estimate can reach < 2 cm, which is in line with the GRACE accuracy of ~ 2 cm globally (Wahr et al., 2006).

Results of the inversion might be compared with those that assimilate GRACE into hydrological models to improve the surface/sub-surface storage compartments. Recent studies over Australia include: DOI:10.1002/2016WR019641; DOI:10.1016/j.advwatres.2017.07.001

R7: We thank for reviewer’s suggestion. We already cited Tian et al. (2017) and approached the same conclusion about the benefit of GRACE on the groundwater estimate, and its limitation of the surface soil moisture.

New references added

Forootan, E., Safari, A., Mostafaie, A., Schumacher, M., Delavar, M., and Awange, J. L.: Large-Scale Total Water Storage and Water Flux Changes over the Arid and Semiarid Parts of the Middle East from GRACE and Reanalysis Products, *Surv. Geophys.*, 38:591-615, doi:10.1007/s10712-016-9403-1, 2017.

Rietbroek, R., Fritsche, M., Brunnabend, S.-E., Daras, I., Kusche, J., Schröter, J., Flechtner, F., and Dietrich, R.: Global surface mass from a new combination of GRACE, modelled OBP and reprocessed GPS data, *J. Geodyn.*, 59 - 60:64 - 71, doi:10.1016/j.jog.2011.02.003, 2012.

Schmeer, M., Schmidt, M., Boschb, W., and Seitz, F.: Separation of mass signals within GRACE monthly gravity field models by means of empirical orthogonal functions, *J. Geodyn.*, 59 - 60:124 - 132, doi:10.1016/j.jog.2012.03.001, 2012.

On the use of GRACE ~~normal equation of intersatellite tracking data~~ for improved estimation of soil moisture and groundwater in Australia

Natthachet Tangdamrongsub¹, Shin-Chan Han¹, Mark Decker², ~~In-Young Yeo¹,
Hyungjun Kim³~~

¹ School of Engineering, University of Newcastle, Callaghan, New South Wales, Australia

² ARC Centre of Excellence for Climate System Science, University of New South Wales, Sydney, New South Wales, Australia

³ ~~Institute of Industrial Science, the University of Tokyo, Tokyo, Japan~~

Abstract

An accurate estimation of soil moisture and groundwater is essential for monitoring the availability of water supply in domestic and agricultural sectors. In order to improve the water storage estimates, previous studies assimilated terrestrial water storage variation (ΔTWS) derived from Gravity Recovery and Climate Experiment (GRACE) into land surface models. However, the GRACE-derived ΔTWS was generally computed from the high level products (e.g., land grid ~~from the Level 3 product~~). The gridded data products are subjected to several drawbacks such as signal attenuation and/or distortion caused by ad hoc posteriori filters, and a lack of error covariance information. ~~The post-processing of GRACE data might lead to the undesired alteration of the signal and its statistical property.~~ To exploit the GRACE information rigorously and negate these limitations, this study uses the fundamental GRACE satellite tracking Level 1B (L1B) data, not the post-processed ΔTWS grid data. ~~Our~~ approach combines the GRACE's least-squares normal equation (full error variance-covariance information) of L1B data with the results from the Community Atmosphere Land Exchange (CABLE) model to improve soil moisture and groundwater estimates. This study demonstrates, for the first time, an importance of using the raw GRACE data. The GRACE-combine (GC) approach is developed for optimal least-squares combination maximizing the strength of the model and observations while suppressing the weaknesses. The approach is applied to estimate the soil moisture and groundwater over 10 Australian river basins and the results are validated against the satellite soil moisture observation and the in-situ groundwater data. We demonstrate the GC approach delivers evident improvement of water storage estimates, consistently from all basins, yielding better agreement at seasonal and inter-annual time scales. Significant improvement is found in groundwater storage while marginal improvement is observed in surface soil moisture estimates likely due to limitation of GRACE's temporal and spatial resolution.

1. Introduction

The changes of Terrestrial Water Storage (ΔTWS) derived from the Gravity Recovery And Climate Experiment (GRACE) data products have been used in the last decade to study global water resources, including groundwater depletion in India and Middle East (Rodell et al., 2009; Voss et al., 2013), water storage accumulation in Canada (Lambert et al., 2013), flood-influenced water storage fluctuation in Cambodia (Tangdamrongsub et al., 2016). The gravity data obtained from GRACE satellites are commonly processed and released in three

Deleted: intersatellite tracking data

Deleted: process

Deleted: The consequence is undesired alteration of ΔTWS data and its statistical property

Deleted: The

48 different product levels (L) that increase in the amount of processing, L1B – satellite tracking
49 data (Wu et al., 2006), L2 – global gravitational Stokes coefficients (Bettadpur, 2012), and
50 L3 – global grids (Landerer and Swenson, 2012). The original (L1B) GRACE information is
51 inevitably altered or sheered due to data processing and successive post-processing filterings,
52 because the error covariance information is not propagated through each post-processing step.

53 The GRACE-derived ΔTWS has been computed widely from the higher-level products (e.g.,
54 L2 and L3) on which various ad hoc post-processing filters were applied (e.g., Gaussian
55 smoothing filter (Jekeli, 1981), destripe filter (Swenson and Wahr, 2006)). ΔTWS obtained
56 from these filters lacks proper error covariance information and is attenuated and distorted.
57 To overcome the signal attenuation in GRACE high-level products, empirical approaches
58 have been developed, including the application of scale factors computed from land surface
59 models (Landerer and Swenson, 2012) to the GRACE L3 products. GRACE uncertainty in
60 high level product is usually unknown or assumed. For example, Zaitchik et al. (2008)
61 derived empirically a global average uncertainty that is variable depending on choices of
62 post-processing filters (Sakumura et al., 2014). Furthermore, GRACE error and sensitivity is
63 dependent on latitudes due to the orbit convergence toward poles (Wahr et al., 2006) and any
64 post-processing filters will alter the GRACE data and their error information. Rigorous
65 statistical error information is of equal importance to derivation of ΔTWS for data
66 assimilation and model calibration (Tangdamrongsub et al., 2017). ΔTWS and its uncertainty
67 estimates should be formulated directly from L1B data considering the complete statistical
68 information.

69 The GRACE information is not fully exploited in many studies. For example, groundwater
70 storage variation (ΔGWS) is often computed by subtracting the soil moisture variation (ΔSM)
71 component simulated by the land surface model from GRACE-derived ΔTWS data (Rodell et
72 al., 2009, Famiglietti et al., 2011), assuming the model ΔSM is error-free. This may result in
73 the inaccurate ΔGWS and the associated error estimate as the uncertainties of GRACE and of
74 the land surface model outputs are neglected in the combination of two noisy data. Several
75 techniques have been developed to separate different signals considering the errors in
76 GRACE and other data (Rietbroek et al., 2012; Schmeer et al., 2012; Forootan et al., 2017).
77 However, the GRACE uncertainty is often derived empirically, not necessarily reflecting the
78 actual GRACE error characteristics. The empirical GRACE errors have been also used in the
79 data assimilation (e.g., Zaitchik et al., 2008; Tangdamrongsub et al., 2015; Tian et al., 2017).
80 For example, Giroto et al. (2016) used L3 product and showed that it was necessary to adjust
81 GRACE observation and its uncertainty in order to make their water storage estimates more
82 accurate. Similarly, Tian et al. (2017) reported the need of applying a scale factor to GRACE
83 uncertainty (from mascon product) in their GRACE assimilation process. It is apparent that
84 the use of post-processed GRACE products often requires data tuning, leading possibly to an
85 integration of incorrect gravity information into the data assimilation system. Some recent
86 studies began to employ the full variance-covariance information in the data assimilation
87 scheme (Eicker et al., 2014, Schumacher et al., 2016; Tangdamrongsub et al., 2017),
88 however, the GRACE signal used were still affected by the post-processing filters.

89 This study aims to use the GRACE information of ΔTWS measurement directly from the raw
90 L1B data. The approach optimally combines the GRACE's least-squares normal equations
91 with the model simulation results from the Community Atmosphere Land Exchange
92 (CABLE, Decker, 2015) to improve ΔSM and ΔGWS estimates. The proposed approach

Deleted: signal separation

Deleted: , which considered

Deleted: complementary

Deleted: in the signal separation process

Deleted: commonly

Deleted: true

Deleted: Similar issue is seen

Deleted: application

Deleted: In data assimilation application, albeit its importance, the GRACE uncertainty is commonly derived empirically not necessarily reflecting the true GRACE error characteristics (e.g., Zaitchik et al., 2008; Tangdamrongsub et al., 2015; Tian et al., 2017).

105 presents three main advantages. Firstly, one can exploit the full GRACE signal and error
 106 information by using the normal equation data sets. Secondly, the approach is developed for
 107 optimal least-squares combination, which maximizes the model and observation strength
 108 while simultaneously suppressing their weaknesses. Finally, the method bypasses empirical,
 109 multiple-step post-processing filters.

110 The main objective of this study is to present the GRACE-combined (GC) approach to
 111 estimate improved ΔSM and ΔGWS at regional scales. We demonstrate our approach applied
 112 to 10 Australian river basins (Fig. 1a). We validate the top layer of ΔSM estimates against the
 113 satellite soil moisture observation (the Advanced Microwave Scanning Radiometer aboard
 114 EOS (AMSR-E), Njoku et al., 2003) over all 10 basins and the ΔGWS estimates against the
 115 in-situ groundwater data available over Queensland and Victoria (Fig. 1b, 1c).

116 This paper is outlined as follows: Firstly, the derivation of GC approach is presented in Sect.
 117 2 while the description of GRACE data processing, including the use of GRACE normal
 118 equation is given in Sect. 3. Secondly, the CABLE modelling is outlined in Sect. 4. This
 119 includes the derivation of model uncertainty based on the quality of precipitation data and the
 120 model parameter inputs. The processing of validation data is also described in Sect. 4.
 121 Thirdly, Sect. 5 presents the result of ΔSM and ΔGWS estimates and comparison to in-situ
 122 data. The long-term trends in the Australian mass variation over the last 13 years is also
 123 investigated in this section.
 124

Deleted: In Sect. 6, the purposed approach is discussed in terms of effectiveness, and data assimilation implementation.

125 2. A method of combining GRACE L1B data with land surface model outputs

126 The statistical information of ΔTWS computed from a model can be written as:

$$127 \quad \tilde{\mathbf{h}} = \mathbf{h} + \boldsymbol{\epsilon}; \boldsymbol{\epsilon} \sim \mathcal{N}(\mathbf{0}, \mathbf{C}), \quad (1)$$

128 where \mathbf{h} is the “truth” (unknown) model state vector while $\tilde{\mathbf{h}}$ is the calculated state vector
 129 characterized with the model error $\boldsymbol{\epsilon}$. The model error is assumed to have zero mean and
 130 covariance \mathbf{C} .

131 The term \mathbf{h} is used to represent a vector including global ΔTWS grid, and terms with a
 132 subscript R (e.g., \mathbf{h}_R , \mathbf{C}_R) is used to represent only a regional set of ΔTWS (for example, in
 133 Australia). As such, the observation equation over a region can be rewritten as:

$$134 \quad \tilde{\mathbf{h}}_R = \mathbf{h}_R + \boldsymbol{\epsilon}; \boldsymbol{\epsilon} \sim \mathcal{N}(\mathbf{0}, \mathbf{C}_R). \quad (2)$$

135 As soil moisture and groundwater are the major components of ΔTWS in Australia (surface
 136 water storage being insignificant), the vector \mathbf{h}_R can be defined as:

$$137 \quad \mathbf{h}_R = [\Delta SM_{top} \quad \Delta SM_{rz} \quad \Delta GWS]^T, \quad (3)$$

138 where ΔSM_{top} , ΔSM_{rz} , ΔGWS represent the vectors of top (surface) soil moisture, root zone
 139 soil moisture, and groundwater storage variations, respectively.

140 A linearized GRACE satellite-tracking observation equation is formulated as:

$$141 \quad \mathbf{y} = \mathbf{A}\mathbf{x} + \mathbf{e}; \mathbf{e} \sim \mathcal{N}(\mathbf{0}, \boldsymbol{\Sigma}), \quad (4)$$

144 where \mathbf{y} is the observation vector containing various kinds of L1B data including the inter-
 145 satellite ranging data, \mathbf{A} is the design (partial derivative) matrix relating the data and the
 146 Earth gravity field variations, \mathbf{x} contains the Stokes coefficients of time-varying geopotential
 147 fields (e.g., Wahr et al., 1998), and \mathbf{e} is the L1B data noise, which has zero mean and
 148 covariance $\mathbf{\Sigma}$. Eq. (4) can be modified explicitly in terms of soil moisture and groundwater
 149 storage variations as:

$$150 \quad \mathbf{y} = \mathbf{A}\mathbf{S}\bar{\mathbf{Y}}\mathbf{H}\mathbf{h} + \mathbf{e}; \mathbf{e} \sim \mathcal{N}(\mathbf{0}, \mathbf{\Sigma}), \quad (5)$$

151 where \mathbf{S} contains a factor used to convert ΔTWS to geopotential coefficients considering the
 152 load Love numbers (e.g., Wahr et al., 1998), $\bar{\mathbf{Y}}$ converts the gridded data into the
 153 corresponding spherical harmonic coefficients, and \mathbf{H} is the operational matrix converting
 154 $\Delta\mathbf{SM}_{top}$, $\Delta\mathbf{SM}_{rz}$, and $\Delta\mathbf{GWS}$ to ΔTWS . This model is based on the assumption that the
 155 GRACE orbital perturbation is a result of ΔTWS variation on the surface, which is very
 156 particular in Australia. For convenience, the term $\mathbf{Y} = \mathbf{S}\bar{\mathbf{Y}}$ is used in the further derivation. If
 157 M is the number of model grid cells, N_{max} is the maximum degree of the geopotential
 158 coefficients, and $L=(N_{max}+1)^2-4$ is the number of geopotential coefficients, the dimension of
 159 \mathbf{Y} , \mathbf{H} , and \mathbf{h} are $L \times M$, $M \times 3M$, and $3M \times 1$, respectively.

160 A least-squares solution of Eq. (5) is given as:

$$161 \quad (\mathbf{H}^T\mathbf{Y}^T\mathbf{A}^T\mathbf{\Sigma}^{-1}\mathbf{A}\mathbf{Y}\mathbf{H})\hat{\mathbf{h}} = \mathbf{H}^T\mathbf{Y}^T\mathbf{A}^T\mathbf{\Sigma}^{-1}\mathbf{y}. \quad (6)$$

162 It can be simplified as:

$$163 \quad \mathbf{H}^T\mathbf{Y}^T\mathbf{N}\mathbf{Y}\mathbf{H}\hat{\mathbf{h}} = \mathbf{H}^T\mathbf{Y}^T\mathbf{c}, \quad (7)$$

164 where $\mathbf{N} = \mathbf{A}^T\mathbf{\Sigma}^{-1}\mathbf{A}$ and $\mathbf{c} = \mathbf{A}^T\mathbf{\Sigma}^{-1}\mathbf{y}$. (The rationales of introducing \mathbf{N} and \mathbf{c} are explained
 165 in the following section). Note that, the above derivations (Eq. (5) – Eq. (7)) are defined with
 166 the global grid of \mathbf{h} . For a regional application, Eq. (7) can be modified as:

$$167 \quad \left[\mathbf{H}_R^T\mathbf{Y}_R^T \mid \mathbf{H}_o^T\mathbf{Y}_o^T \right] \mathbf{N} \begin{bmatrix} \mathbf{Y}_R\mathbf{H}_R \\ \mathbf{Y}_o\mathbf{H}_o \end{bmatrix} \begin{bmatrix} \hat{\mathbf{h}}_R \\ \hat{\mathbf{h}}_o \end{bmatrix} = \left[\mathbf{H}_R^T\mathbf{Y}_R^T \mid \mathbf{H}_o^T\mathbf{Y}_o^T \right] \mathbf{c}, \quad (8)$$

168 where the subscript R indicates the grid ΔTWS only in a region of interest, and o for the rest
 169 of the globe. If the number of the model grid cells associated with R is J and that of the
 170 outside cells is $M-J$. As such, the dimensions of \mathbf{Y}_R , \mathbf{H}_R , $\hat{\mathbf{h}}_R$, \mathbf{Y}_o , \mathbf{H}_o , $\hat{\mathbf{h}}_o$ are $L \times J$, $J \times 3J$, $3J \times 1$,
 171 $L \times (M-J)$, $(M-J) \times 3(M-J)$, $3(M-J) \times 1$, respectively. The dimension of \mathbf{N} and \mathbf{c} remain
 172 unchanged, since they are essentially from the normal equations of the original GRACE L1B
 173 data (to be discussed in the following section).

174 From Eq. (8), the normal equations associated with ΔTWS in the region of interest can then
 175 be written as

$$176 \quad \mathbf{H}_R^T\mathbf{Y}_R^T\mathbf{N}\mathbf{Y}_R\mathbf{H}_R\hat{\mathbf{h}}_R = \mathbf{H}_R^T\mathbf{Y}_R^T\mathbf{c} - \mathbf{H}_R^T\mathbf{Y}_R^T\mathbf{N}\mathbf{Y}_o\mathbf{H}_o\hat{\mathbf{h}}_o \quad (9)$$

177 or

$$178 \quad \mathbf{N}_R\hat{\mathbf{h}}_R = \mathbf{c}_R \quad (10)$$

179 where $\mathbf{N}_R = \mathbf{H}_R^T\mathbf{Y}_R^T\mathbf{N}\mathbf{Y}_R\mathbf{H}_R$ and $\mathbf{c}_R = \mathbf{H}_R^T\mathbf{Y}_R^T\mathbf{c} - \mathbf{H}_R^T\mathbf{Y}_R^T\mathbf{N}\mathbf{Y}_o\mathbf{H}_o\hat{\mathbf{h}}_o$. As seen, Eq. (9) is the
 180 regional representation of Eq. (7) where only the grid cells inside the study region are used,

Deleted: the

182 while the contribution from the grid cells outside the region needs to be removed or
 183 corrected. Combining the normal equation of Eq. (2) and Eq. (10), the optimal combined
 184 solution of $\hat{\mathbf{h}}_R$ can be resolved as follows:

$$185 \quad \hat{\mathbf{h}}_R = (\mathbf{C}_R^{-1} + \mathbf{N}_R)^{-1} (\mathbf{C}_R^{-1} \tilde{\mathbf{h}}_R + \mathbf{c}_R) \quad (11)$$

186 The computation of model covariance matrix \mathbf{C}_R will be discussed in Sect. 4.2. The posteriori
 187 covariance of $\hat{\mathbf{h}}_R$ can be estimated as follows:

$$188 \quad \hat{\Sigma} = (\mathbf{C}_R^{-1} + \mathbf{N}_R)^{-1}, \quad (12)$$

189 and the uncertainty estimate of $\hat{\mathbf{h}}_R$ is simply calculated as:

$$190 \quad \sigma_{\hat{\mathbf{h}}} = \sqrt{\text{diag}(\hat{\Sigma})}, \quad (13)$$

191 where $\text{diag}()$ represents the diagonal element of the given matrix.

192

193 3. GRACE data

194 3.1 GRACE least-squares normal equations

195 In this study, the least-squares normal equations are obtained from the ITSG-Grace2016
 196 products (Mayer-Gürr et al, 2016; [https://www.tugraz.at/institute/ifg/downloads/gravity-field-](https://www.tugraz.at/institute/ifg/downloads/gravity-field-models/itsg-grace2016)
 197 [models/itsg-grace2016](https://www.tugraz.at/institute/ifg/downloads/gravity-field-models/itsg-grace2016)) between January 2003 and March 2016. All L1B data including KBR
 198 inter-satellite tracking data, attitude, accelerometer, GPS based kinematic orbit data and
 199 AOD1B corrections are reduced in terms of the normal equations. These data products are
 200 usually used to compute the Earth's geopotential field to the maximum harmonic degree and
 201 order of 90, or at a spatial resolution of ~220 km. The products contain the information of the
 202 normal matrix \mathbf{N} and the vector \mathbf{c} (as shown in Eq. (7)) as well as the a-priori time-varying
 203 gravity field coefficients predicted with the GOCO05s solution (Mayer-Gürr et al., 2015).
 204 Note that the solution of the ITSG-Grace2016 normal equation is the anomalous geopotential
 205 coefficient vector ($\Delta\mathbf{x}$), which is referenced to the a-priori time-varying gravity field (\mathbf{x}_0),
 206 through:

$$207 \quad \mathbf{N} \Delta\mathbf{x} = \mathbf{d} \quad (14)$$

208 where \mathbf{d} and \mathbf{x}_0 are given. To obtain a complete gravity field variation between the study
 209 period (\mathbf{x} term in in Eq. (4)), the a-priori time-varying gravity field, \mathbf{x}_0 is firstly restored to
 210 Eq. (14), and the mean gravity field ($\bar{\mathbf{x}}_0$) computed from all \mathbf{x}_0 between January 2003 and
 211 March 2016 is then removed as follows:

$$212 \quad \mathbf{N} (\Delta\mathbf{x} + \mathbf{x}_0 - \bar{\mathbf{x}}_0) = \mathbf{d} + \mathbf{N}(\mathbf{x}_0 - \bar{\mathbf{x}}_0) \quad (15)$$

$$213 \quad \mathbf{N} \mathbf{x} = \mathbf{d} + \mathbf{N}(\mathbf{x}_0 - \bar{\mathbf{x}}_0) \quad (16)$$

214 Therefore, in Sect. 2 (e.g., Eq. (7) – (11)), the matrix \mathbf{N} remains unchanged while the vector \mathbf{c}
 215 can be simply replaced by $\mathbf{c} = \mathbf{d} + \mathbf{N}(\mathbf{x}_0 - \bar{\mathbf{x}}_0)$.

216

217 3.2 GRACE-derived ΔTWS products

218 Two monthly GRACE-derived ΔTWS products are also used, the CNES/GRGS Release 3
219 (RL3) (GRGS for short, Lemoine et al., 2015) and the JPL RL05M mascon-CRI version 2
220 product (mascon for short, Watkins et al., 2015; Wiese et al., 2016). The GRGS solution
221 provides ΔTWS at $1^\circ \times 1^\circ$ globally, derived from the Earth's geopotential coefficients up to the
222 maximum degree and order 80, and no filter nor scale factor is applied (L2 data product).
223 Mascon provides ΔTWS at equal-area 3° spherical cap grid globally. In contrast to the GRGS
224 solution, the mascon uses a gain factor derived from the land surface model (LSM) to restore
225 mitigated signals and reduce leakage errors (L3 data products) (Watkins et al., 2015; Wiese et
226 al., 2016). Additionally, mascon provides the ΔTWS uncertainty together with the solution.
227 The uncertainty is computed based on several geophysical models (see Watkins et al. (2015)
228 and Wiese et al. (2016) for more details). The uncertainty information is not available in the
229 GRGS product.

230 The ΔTWS products are obtained between January 2003 and March 2016. The GRGS
231 solution is retrieved from [http://grgs.obs-mip.fr/grace/variable-models-grace-lageos/grace-](http://grgs.obs-mip.fr/grace/variable-models-grace-lageos/grace-solutions-release-03)
232 [solutions-release-03](http://grgs.obs-mip.fr/grace/variable-models-grace-lageos/grace-solutions-release-03) while the mascon is from [http://grace.jpl.nasa.gov/data/get-](http://grace.jpl.nasa.gov/data/get-data/jpl_global_mascons)
233 [data/jpl_global_mascons](http://grace.jpl.nasa.gov/data/get-data/jpl_global_mascons). After retrieval, the long-term mean value between January 2003
234 and March 2016 is computed and subtracted from the monthly products. To be consistent
235 with CABLE grid spacing (see Sect. 4), the spatial resolution of two datasets are resampled to
236 $0.5^\circ \times 0.5^\circ$ using the nearest grid values.

237 In this study, these two independent GRACE solutions are used for two main reasons:

- 238 1. To obtain the ΔTWS values outside Australia. As shown in Eq. (9), the $\hat{\mathbf{h}}_o$ vector
239 needs to be known, which can be from the GRACE-derived ΔTWS solution. We use
240 the GRGS solutions as the GRGS solution provides ΔTWS at a spatial resolution
241 comparable to the normal equation data.
- 242 2. To compare with the ΔTWS estimates from our approaches. Both GRGS and [JPL](#)
243 mascon solutions are used to compare and validate our ΔTWS estimates.

246 4. Hydrology model and validation data

247 4.1 Model setup

248 The extensive description of the CABLE model is given in Decker (2015) and Ukkola et al.
249 (2016). This section describes the model setup and specific changes applied for this study.
250 CABLE can be used to estimate soil moisture and groundwater in terms of volumetric water
251 content every 3 hours at a $0.5^\circ \times 0.5^\circ$ spatial resolution. The soil moisture and groundwater
252 storage can be simply computed by multiplying the estimates with thicknesses of various
253 layers. For soil moisture, the thickness of 6 soil layers is 0.022, 0.058, 0.154, 0.409, 1.085,
254 and 2.872 m, from top to bottom, respectively. The thickness of the groundwater layer is
255 modelled to be 20 m uniformly. Recalling Eq. (3), ΔSM_{top} is defined as the soil moisture
256 storage variation at the top 0.022 m thick layer, while ΔSM_{rz} is the variation accumulated
257 over the second to the bottom soil layers (depth between 0.022 m and 4.6 m).

258 CABLE is initially forced with the data from the Global Soil Wetness Project Phase 3
259 (GSWP3), which is currently available until December 2010 (<http://hydro.iis.u->

Deleted: c

Deleted: (Dirmeyer et al., 2011; <http://hydro.iis.u-tokyo.ac.jp/GSWP3>)

263 tokyo.ac.jp/GSWP3, <https://doi.org/10.20783/dias.501>). We replace GSWP3 forcing data
 264 with GLDAS data (Rodell et al., 2004) to compute the water storage changes to 2016. The
 265 forcing data used in CABLE are precipitation, air temperature, snowfall rate, wind speed,
 266 humidity, surface pressure, and short-wave and long-wave downward radiations. To
 267 investigate the impact of different forcing data, the offline sensitivity study is conducted by
 268 comparing the water storage estimates computed using:

- 269 1. All 8 forcing data components of GSWP3,
- 270 2. GSWP3 data with replacing one component obtained from GLDAS forcing data.

271 It is found that the water storage estimate is most sensitive to the replacement of precipitation
 272 data, as expected, and relatively less sensitive to the change of other forcing components. We
 273 use the GLDAS forcing data in this study and also further test 7 different precipitation data
 274 products (see more details in Sect. 4.2). The forcing data are up/down sampled to a $0.5^\circ \times 0.5^\circ$
 275 spatial grid to reconcile with the CABLE spatial resolution.
 276

277 4.2 Model uncertainty

278 In this study, the CABLE uncertainty is derived from 210 ensemble estimates associated with
 279 different forcing data and model parameters. The 7 different precipitation products (see Table
 280 1) are used to run the model independently. Most products are available to present day while
 281 GSWP3, Princeton, and MERRA are only available until December 2010, December 2012,
 282 and February 2016, respectively. For each precipitation forcing, 30 ensembles are generated
 283 by perturbing the model parameters within $\pm 10\%$ of the nominal values. The perturbed size
 284 of 10% is similar to Dumedah and Walker (2014). Based on the CABLE structure, the ΔSM
 285 and ΔGWS estimates are most sensitive to the model parameters listed in Table 2. For
 286 example, the fractions of clay, sand, and silt (f_{clay} , f_{sand} , f_{silt}) are used to compute soil
 287 parameters including field capacity, hydraulic conductivity, and soil saturation which mainly
 288 affect soil moisture storage. Similarly, the drainage parameters (e.g., q_{sub} , f_p) control the
 289 amount of subsurface runoff, which has a direct impact on root zone soil moisture and
 290 groundwater storages.

291 From ensemble generations, total $K = 210$ sets of the ensemble water storage estimates (\mathbf{h}_e)
 292 are obtained:

$$293 \quad \mathcal{H}_R = [\mathbf{h}_e|_{k=1} \quad \mathbf{h}_e|_{k=2} \quad \mathbf{h}_e|_{k=3} \quad \dots \quad \mathbf{h}_e|_{k=K}] \quad (17)$$

294 and the mean value of \mathcal{H}_R is computed as follows:

$$295 \quad \tilde{\mathbf{h}}_R = \frac{1}{K} \sum_{k=1}^K \mathbf{h}_e|_k \quad (18)$$

296 Note that due to the absence of GSWP3, Princeton, and MERRA data, the number of
 297 ensembles reduce to $K = 180$ after December 2010, $K = 150$ after December 2012, and $K =$
 298 120 after February 2016, respectively. The GC approach assumes that model errors are
 299 normally distributed with zero mean. Any violation of this assumption will yield a bias in the
 300 combined solutions. Therefore, the mean value is removed from each ensemble member,
 301 $\mathcal{H}_R' = \mathcal{H}_R - \tilde{\mathbf{h}}_R$, and the error covariance matrix of the model is empirically computed as:

$$302 \quad \mathbf{C}_R = \mathcal{H}_R' (\mathcal{H}_R')^T / (K - 1) \quad (19)$$

303 The $\tilde{\mathbf{h}}_R$ (Eq. (18)) and \mathbf{C}_R (Eq. (19)) terms can be directly used in Eq. (11).

304 Note that the sampling error caused by finite sample size might lead to spurious correlations
305 in the model covariance matrix (Hamill et al., 2001). The effect can be reduced by applying
306 an exponential decay with a particular spatial correlation length to \mathbf{C}_R . In this study, the
307 correlation length is determined based on the empirical covariance of model estimated
308 ΔTWS . The covariance function of ΔTWS is firstly assumed isotropic, and it is computed
309 empirically based on the method given in Tscherning and Rapp (1974). The distance where
310 the maximum value of the variance decreases to half is defined as the correlation length. The
311 obtained values vary month-to-month, and the mean value of 250 km is used in this study.

312 It is emphasized that the model omission error caused by imperfect modelling of hydrological
313 process within the LSM is not taken into account in the above description. The omission error
314 may increase the model covariance and introduce a bias as well. We account for the omission
315 error by increasing 20% of the model covariance. (i.e., multiplying \mathbf{C}_R by 1.2). We determine
316 such omission error based on trial-and-error such that it increases the model error (due to the
317 omission error) but not exceeds the model error value reported by Dumedah and Walker
318 (2014). We acknowledge that this is only a simple practical way of accounting for the
319 omission error into the total model error.

321 4.3 Validation data

322 4.3.1 Satellite soil moisture observation

323 The satellite observed surface soil moisture data is obtained from the Advanced Microwave
324 Scanning Radiometer-Earth Observing System (AMSR-E) using the Land Parameter
325 Retrieval Model (Njoku et al., 2003). The observation is used to validate our estimates of top
326 soil moisture changes (ΔSM_{top}). The AMSR-E product provides volumetric water content in
327 the top layer derived from a passive microwave data (from NASA EOS Aqua satellite) and
328 forward radiative transfer model. In this study, the level 3 product, available daily between
329 June 2002 and June 2011 at $0.25^\circ \times 0.25^\circ$ spatial resolution is used (Owe et al., 2008). The
330 measurements from ascending and descending overpasses are averaged for each frequency
331 band (C and X). Then, the monthly mean value is computed by averaging the daily data
332 within a month. To obtain the variation of the surface soil moisture, the long-term mean
333 between June 2002 and June 2011 is removed from the monthly data. Regarding the different
334 depth measured in CABLE and AMSR-E, the CDF-matching technique (Reichle and Koster,
335 2004) is used to reduce the bias between the top soil moisture model and the observation. The
336 CDF is built using the 2003-2004 data, and it is used for the entire period. There is no
337 satellite observed or ground measured root zone soil moisture data for meaningful
338 comparison with our results, particularly at continental scale. Validation of ΔSM_{rz} at regional
339 and continental scales is currently unachievable due to a complete lack of observations at this
340 spatial scale.

342 4.3.2 In-situ groundwater

343 The in-situ groundwater level from bore measurements are obtained from 2 different ground
344 observation networks (see Fig. 1). The data in Queensland are obtained from Department of

Deleted: assume

Deleted: for such model error

Deleted: assume

Deleted: the

Deleted: this way

Deleted: t

Deleted: o be a good compromise between

Deleted: ing of

Deleted: and

Deleted: ing

Deleted: upper limit of the

Deleted: suggested

Deleted: However, it should be noted that t

Deleted: assumption has a limitation of representing the error characteristic and more investigation is needed in order to acquire a more realistic omission error

Deleted: cooperating

Deleted: Since t

363 Natural Resources and Mines (DNRM) while the data in Victoria is from Department of
364 Environment and Primary Industries (DWPI). More than 10,000 measurements are available
365 from each network, but the data gap and outliers are present. Therefore, the bore
366 measurement is firstly filtered by removing the sites that present no data or data gap longer
367 than 30 months during the study period.

368 To obtain the monthly mean value, the hourly or daily data are averaged in a particular
369 month. The outliers are detected and fixed using the Hampel filter (Pearson, 2005) where the
370 remaining data gaps are filled using the cubic spline interpolation. To obtain the groundwater
371 level variation, the long-term mean groundwater level computed between the study period is
372 removed from the monthly values. The groundwater level variation (ΔL) is then converted to
373 ΔGWS using $\Delta GWS = S_y \cdot \Delta L$, where S_y is specific yield. Based on Chen et al. (2016), $S_y =$
374 0.1 is used for the Victoria network. Specific yields of Queensland's network have been
375 found ranging from 0.045 (Rassam et al., 2013) to 0.06 (Welsh 2008), and an averaged $S_y =$
376 0.05 is used in this study. Finally, the mean value computed from all data (in each network) is
377 used to represent the in-situ data of the network.

378

379 5. Results

380 5.1 Model-only performance

381 We study the model ΔTWS changes under different meteorological forcing and land
382 parameterization. Total 210 estimates of monthly TWS (sum of SM_{top} , SM_{rz} , and GWS) are
383 obtained between January 2003 and March 2016 from the ensemble run based on 7 different
384 precipitation inputs. Then, the averaged values of the TWS estimates are computed from the
385 30 precipitation-associated ensemble members. This results in 7 sets of monthly mean TWS
386 estimates from 7 different precipitation data. For each set, the monthly ΔTWS is computed by
387 removing the long-term mean computed between January 2003 and March 2016.

388 The precipitation-based ΔTWS are then compared with the GRACE-mascon solution (see
389 Sect. 3.2) over 10 different Australian basins. The comparison is carried out between January
390 2003 and March 2016. Due to the availability of the data, the periods used are shorter in cases
391 of GSWP3, Princeton, and MERRA precipitation (see Table 1). The metric used to evaluate a
392 goodness of fit between CABLE run and GRACE mascon estimates is the Nash-Sutcliffe (NS)
393 coefficient (see Eq. (A1)) (Fig. 2).

394 Figure 2 demonstrates CABLE ΔTWS varies noticeably by precipitation as well as locations.
395 The area-weighted average values (see Eq. (A2)) computed from Princeton, GSWP3, and
396 TRMM yields the model ΔTWS reasonably agreeing with GRACE by giving the NS
397 coefficient greater than 0.45, while MERRA, PERSIANN, and GLDAS show $NS = \sim 0.3$. The
398 less agreement is mainly due to the quality of rainfall estimates over Australia. The NS of
399 ECMWF is around 0.4.

400 All model ensembles are consistent with the GRACE data over Timor Sea and inner parts of
401 Australia (e.g., LKE, MRD, NWP) where the NS value can reach as high as 0.9 (see e.g.,
402 TRMM over TIM). On the contrary, the less agreement is found mostly over the coastal
403 basins. Very small or even negative NS values indicate the misfit between CABLE and
404 GRACE mascon solutions, and they are observed over Indian Ocean (see GLDAS), North

405 East Coast (see GSWP3, PERSIANN, TRMM), South East Coast (see MERRA, TRMM),
406 South West Coast (see GSWP3, GLDAS, MERRA), and South West Plateau (see MERRA).

407 By averaging all ΔTWS estimates from seven different precipitation datasets, the mean-
408 ensemble estimate (MN) delivers the best agreement with GRACE as seen by the highest
409 average NS value (MN of AVG = 0.55) among all ensembles. Particularly, NS values are
410 greater than 0.4 in all basins and no negative NS values are presented in MN. In average, it
411 can be clearly seen that using the mean value (MN) is a viable option to increase the overall
412 performance of the ΔTWS estimates. Therefore, only CABLE MN result will be used in
413 further analyses. The comparison with the GRGS GRACE solution was also evaluated (not
414 shown here) and the overall results are similar to Fig. 2.

415

416 5.2 Impact of GRACE on storage estimates

417 5.2.1 Contribution of GRACE

418 This section investigates the impact of the GC approach on the estimates of various water
419 storage components. The ΔTWS estimate obtained from the GC approach is demonstrated in
420 Sect. 5.1, by comparing with the independent GRACE mascon solution. Figure 2 shows the
421 GC result yields the highest NS values in all basins, outperforming all other CABLE runs. In
422 average (AVG), the NS value increases by ~35% (0.55 to 0.74) from the MN case. The
423 similar behaviour is also seen when compared with the GRGS GRACE solution (not shown);
424 the average NS value increases from 0.50 to 0.74. This is not surprising as the GC approach
425 uses the fundamental GRACE tracking data as GRACE mascon and GRGS solutions do.
426 Improvement of NS coefficient indicates merely the successfulness of integrating GRACE
427 data and the model estimates.

428 Figure 3 shows the GC results of ΔTWS as well as ΔSM_{top} , ΔSM_{rz} , and ΔGWS in different
429 basins. The monthly time-series and the de-seasonalized time-series are shown. In general,
430 GRACE tends to increase ΔTWS when the model ΔTWS (MN) is predicted to be
431 underestimated (see e.g., LKE, MRD, NWP, SWP, TIM between 2011 and 2012) and by
432 decrease ΔTWS when determined to be overestimated (see all basins between 2008 and
433 2010). A clear example is seen over Gulf of Carpentaria (Fig. 3d), where CABLE
434 overestimates ΔTWS and produces phase delay between 2008 and 2010. The over estimated
435 amplitude and phase delay seen in CABLE ΔGWS during this above period (Fig. 3c) is
436 caused by an overestimation of soil and groundwater storage. The positively biased soil and
437 groundwater storage causes a phase delay by increasing the amount of time required for the
438 subsurface drainage (baseflow) to reduce to soil and groundwater stores. The overestimation
439 of water storage is the result of overestimated precipitation or underestimated
440 evapotranspiration. The amplitude and phase of the water storage estimate are adjusted
441 toward GRACE observation in the GC approach.

442 The impact of GRACE varies across the individual storage as well as across the geographical
443 location (climate regime). In general, the major contributors to ΔTWS are ΔSM_{rz} and ΔGWS .
444 Due to a small store size (only ~2 cm thick), ΔSM_{top} contributes only ~2 % to ΔTWS . As
445 such, ΔSM_{rz} , and ΔGWS have greater variations, which commonly lead to greater uncertainty
446 compared to ΔSM_{top} , and therefore, the stores anticipate greater shares from the GRACE

Deleted: 7

448 update. This behaviour is seen over all basins where the differences between CABLE-
449 simulated and GC ΔSM_{rz} , and ΔGWS estimates are greater (compared to ΔSM_{top}).

450 Furthermore, the impact of GRACE on ΔSM_{rz} , and ΔGWS is different across the continent.
451 For example, over central and southern Australia (see e.g., LKE, MRD, NWP, SWP), the dry
452 climate is responsible for a small amount of groundwater recharge and most of the infiltration
453 is stored in soil compartments. In this climate condition, ΔSM_{rz} amplitude is significantly
454 larger than ΔGWS and it plays a greater role in ΔTWS , and consequently, the GRACE
455 contribution is mostly seen in ΔSM_{rz} component. Different behaviour is seen over the
456 northern Australia (GOC, NEC, TIM) where ΔGWS amplitude are greater (~40 % of ΔTWS)
457 compared to other basins (only ~17 % of ΔTWS). This is due to the sufficient amount of
458 rainfall over the wet climate region, replenishing groundwater recharges and resulting in
459 greater variability in ΔGWS . Therefore, compared to the dry climate basin, the GRACE
460 contributes to ΔGWS over these basins by the larger amount.
461

462 5.2.2 Impact on long-term trend estimates

463 The spatial patterns of the long-term trends of water storage changes over January 2003 and
464 March 2016 are analysed before and after applying the GC approach (Fig. 5). For
465 comparison, the long-term trends of ΔTWS derived from the mascon and GRGS solutions are
466 also shown (Fig. 5a, 5b). From Fig. 5d, GRACE effectively changes the long-term trend
467 estimates in most basins in a way the spatial pattern of the ΔTWS trend of the GC solution
468 consistent to the mascon and GRGS solutions, while satisfying the model processes and
469 keeping the spatial resolution. The trend of ΔSM_{top} is insignificant (Fig. 5e) and the GC
470 approach does not change (Fig. 5f). The largest adjustment is seen in ΔSM_{rz} and ΔGWS
471 components, to be consistent with the GRACE data in most basins (Fig. 5h, 5j).

472 GRACE shows significant changes in the ΔTWS trend estimates particularly over the
473 northern and western parts of the continent. The model estimates around the Gulf of
474 Carpentaria basin show a strong negative trend that is inconsistent from the GRACE data. It
475 is found that underestimated precipitation after 2012 is likely the cause of such an
476 incompatible negative trend (see Fig. 3d). Applying the GC approach clearly improves the
477 trend (Fig. 5c vs. 5d). The other example is seen over the western part of the continent (see
478 rectangular area in Fig. 5c, 5d) where the averaged long-term trend of ΔTWS was predicted
479 to be -0.4 cm/year but changed to be -1.2 cm/year (see also Sect. 5.4) by the GC approach.
480 The precipitation over the western Australia is understood to be overestimated after 2012,
481 evidently seen by that the model ΔTWS is always greater than the GC solution (see e.g., Fig.
482 3h, 4d, 4p). The GC approach reveals that the water loss over the western Australia is at least
483 twice greater than what has predicted by the CABLE model.

484 In addition, the shortage of water storage in the south-eastern part of the continent from the
485 millennium drought (McGrath et al., 2012) has been recovered (seen as a positive water
486 storage trend in Fig. 5) after the rainfall between 2009 and 2012, while the western part is
487 still drying out (seen as negative trends). The trend estimates in terms of mass change is
488 discussed in more detail in Sect. 5.4.
489

490 5.2.3 Reduction of uncertainty

491 Influenced by climate pattern, the uncertainty of water storage estimates significantly varies
492 across Australia. The uncertainty of the model estimate is computed from the variability
493 induced by different precipitation and model parameters while the uncertainty of GC solution
494 is computed using Eq. (13). As expected, larger uncertainties are observed in ΔSM_{rz} and
495 ΔGWS than in ΔSM_{top} (an order of magnitude smaller) since ΔSM_{top} is smaller than others
496 (Fig. 6). Over the wet basins, larger amplitude of the water storage leads to larger uncertainty,
497 seen over Gulf of Carpentaria, North East Coast, South East Coast, and Timor Sea where the
498 CABLE-simulated ΔTWS uncertainty is approximately 28 % larger than other basins. The
499 smaller uncertainty is found over the dry regions (e.g., LKE, SWP). In most basins, the
500 uncertainty of ΔSM_{rz} is larger than the ΔGWS , except the wet basins (e.g., GOC, NEC, TIM)
501 where the greater groundwater recharge leads to a larger uncertainty of ΔGWS .

502 Figure 6 demonstrates how much the formal error of each of storage components is reduced
503 by the GC approach. Overall, the estimated CABLE uncertainties averaged over all basins
504 (AVG) are 0.2, 4.0, 4.0, and 5.7 cm for ΔSM_{top} , ΔSM_{rz} , ΔGWS , and ΔTWS , respectively.
505 With the GC approach, the uncertainties of ΔSM_{top} , ΔSM_{rz} , ΔGWS , and ΔTWS decrease by
506 approximately 26%, 35%, 39%, and 37%, respectively.

507 It is worth mentioning that the model uncertainty is mainly influenced by the meteorological
508 forcing data. The uncertainty of precipitation derived from seven different precipitation
509 products is shown in Fig. 6e. The spatial pattern of the precipitation uncertainty is correlated
510 with the uncertainty of water storage estimates. The larger water storage uncertainty is
511 deduced from the larger precipitation uncertainty. The quality of precipitation forcing data is
512 found to be an important factor to determine the accuracy of water storage computation.
513

Deleted: 7

514 **5.3 Comparison with independent data**

515 **5.3.1 Soil moisture**

516 The ΔSM_{top} estimates are compared with the AMSR-E derived soil moisture. The processing
517 of AMSR-E data is described in Sect 4.3.1. The performance is assessed using Nash-Sutcliffe
518 coefficients, given in Table 3. In general, CABLE (MN) shows a good performance in the top
519 soil moisture simulation showing NS value of >0.4 for most of the basins. The top soil
520 moisture estimate shows slightly better agreement with the C-band measurement of the
521 AMSR-E product. This is likely caused by the greater emitting depth of the C-band
522 measurement (~ 1 cm), which is closer to the depth of the top soil layer (~ 2 cm) used in this
523 study (Njoku et al., 2003).

524 The GC approach leads to a small bit of improvement of the top soil estimate consistently
525 from C- and X-band measurements and from all basins. No degradation of the NS value is
526 observed in the GC solutions. The largest improvement is seen over LKE and NEC, where
527 NS increases by 10 – 15%. For other regions, the change in the NS coefficient may be
528 incremental.
529

530 **5.3.2 Groundwater**

531 The ΔGWS estimates from the model and the GC method are compared with the in situ data
532 obtained from 2 different ground networks in Queensland and Vitoria. For each network, all

534 ΔGWS data inside the groundwater network boundary (see polygons in Fig. 1) are used to
535 compute the average ΔGWS time series. From the comparison given in Fig. 7, it is found that
536 the GC solutions of ΔGWS follows the overall inter-annual pattern of CABLE but with a
537 considerably larger amplitude. This results in a better agreement with the in situ ΔGWS data
538 seen from both networks. The NS coefficient of ΔGWS between the estimates and the in situ
539 data are given in Table 4. The CABLE ΔGWS performs significantly better in Queensland
540 (NS = ~ 0.5) than Victoria (NS = ~ 0.3). Significant improvement is found from the GC
541 solutions in both networks, where the NS value increases from 0.5 to 0.6 ($\sim 22\%$) in
542 Queensland and from 0.3 to 0.6 ($\sim 85\%$) in Victoria. Even greater improvement is seen when
543 the inter-annual patterns are compared. The NS value increase from 0.5 to 0.7 ($\sim 32\%$), and
544 0.4 to 0.8 ($\sim 93\%$) in Queensland and Victoria, respectively.

545 The comparison of the long-term trend of ΔGWS is also evaluated. The estimated trends in
546 Queensland and Victoria are given in Table 4. Beneficially from the GC approach, the ΔGWS
547 trend is improved by approximately 20% (from 0.4 to 0.6, compared to 1.6 cm/year) in
548 Queensland. Increasing of ΔGWS is mainly influenced by the large amount of rainfall during
549 the 2009 – 2012 La Niña episodes (see Fig. 7a). In Victoria, significant improvement of
550 ΔGWS trend by about 76% (from 0.1 to -0.2 , compared to -0.3 cm/year) is observed.
551 Similar improvement of long-term trend estimates is seen in de-seasonalized time series
552 (improves by $\sim 15\%$ in Queensland and by $\sim 74\%$ in Victoria). Decreasing of ΔGWS in
553 Victoria is mainly due to the highly-demanded groundwater consumption by agriculture and
554 domestic activities (van Dijk et al., 2007; Chen et al., 2016). As the groundwater
555 consumption is not parameterized in CABLE, the decreasing of ΔGWS estimate cannot
556 properly captured in the model simulation. Applying GC approach effectively reduces the
557 model deficiency and improves the quality of the groundwater estimations.
558

559 **5.4 Assessment of mass variation in the past 13 years**

560 Australia experiences significant climate variability; for example the millennium drought
561 starting from late '90 (Van Dijk et al., 2013) and extremely wet condition during several La
562 Niña episodes (Trenberth 2012; Han 2017). These periods are referred as “Big Dry” and “Big
563 Wet” (Ummenhofer et al., 2009; Xie et al., 2016). To understand the total water storage
564 (mass) variation influenced by these two distinct climate variabilities, the water storage
565 change obtained from the GC approach during Big Dry and Big Wet is separately
566 investigated over 10 basins. The time window between January 2003 and December 2009 is
567 defined as the Big Dry period while between January 2010 and December 2012 is defined as
568 the Big Wet period following Xie et al. (2016). In each period, the long-term trends of GC
569 estimates of ΔTWS , ΔSM_{top} , ΔSM_{rz} , and ΔGWS are firstly calculated. Then, the total water
570 storage variation (in meter) is simply obtained by multiplying the long-term trend (in m/year)
571 with the number of years in the specific period, 7 years for Big Dry and 3 years for Big Wet.
572 To obtain the mass variation, the water storage variation is multiplied by the area of the basin
573 and the density of water (1000 kg/m^3). The estimated mass variations during Big Dry and Big
574 Wet are displayed in Fig. 8. The long-term mass variation of the entire period (January 2003
575 – March 2016) is also shown.

576 During Big Dry (2003 – 2009), a significant loss of total storage (40 – 60 Gton over 7 years)
577 is observed over LKE, MRD, NWP, and SWP basins. The largest groundwater loss of >20

578 Gton is found from LKE and MRD. No significant change is observed over the tropical
579 climate regions (e.g., GOC, NEC). The mass loss mostly occurs in the root zone and
580 groundwater compartments where the sum of ΔSM_{rz} and ΔGWS explains more than 90% of
581 the ΔTWS value. The mass loss is also observed in ΔSM_{top} but >10 times smaller than
582 ΔSM_{rz} and ΔGWS .

583 During Big Wet (2010 – 2012), the basins like LKE, MRD and TIM exhibit the significant
584 total storage gain of >100 Gton. The gain is particularly larger in ΔSM_{rz} over the basins that
585 experienced the significant loss during Big Dry. For example, over LKE and MRD, the gain
586 of ΔSM_{rz} is approximately 2 – 3 times greater than ΔGWS . It implies that most of the
587 infiltration (from the 2009 – 2012 La Niña rainfall) is stored as soil moisture through the long
588 drought period, and that the groundwater recharge is secondary to the ΔSM_{rz} increase.

589 The opposite behaviour is observed over the basins (such as NEC and GOC) that experienced
590 mass gain during Big Dry. The water storage gain is greater in ΔGWS compared to ΔSM_{rz} . In
591 NEC, ΔGWS gain is ~8 times larger than ΔSM_{rz} during Big Wet. The soil compartment may
592 be saturated during Big Dry and additional infiltration from the Big Wet precipitation leads to
593 an increased groundwater recharge. The ΔSM_{rz} loss observed over GOC is simply caused by
594 the timing selection of Big Wet period, which ends earlier (~2011) in GOC than in other
595 basins. The ΔSM_{rz} gain becomes ~26 Gton if the Big Wet period is defined as 2008 – 2011.
596 During the post-Big Wet period (2012 and afterwards), the decreasing trend of water storage
597 is observed from all basins (see Fig. 3, 4). This is mainly caused by the decrease in
598 precipitation after 2012 and by gradual water loss through evapotranspiration (Fasullo et al.,
599 2013).

600 The overall water storage change in the last 13 years demonstrates that the severe water loss
601 from most basins during Big Dry (the millennium drought) is balanced with the gain during
602 Big Wet (the La Niña). The negative ΔTWS estimated during Big Dry becomes positive in
603 LKE, MRD, and SEC and less negative in TIM, and the greatest gain is observed from NEC
604 by ~50 Gton during 13 year-period (see Fig. 8c). However, the water mass loss is still
605 detected over the western basins (e.g., IND, NWP, SWP, SWC), and their magnitudes are
606 even larger than the mass loss during Big Dry. For example, the greatest ΔTWS loss of ~79
607 Gton is observed over NWP, which is ~25 Gton greater than the loss during Big Dry (see Fig.
608 8a and 8c). The basin is less affected by the La Niña, and the rainfall during Big Wet is
609 clearly inadequate to support the water storage recovery in the basin. Rainfall deficiency also
610 reduces the groundwater recharge, resulting in even more decreasing of ΔGWS , compared to
611 the Millennium Drought period (see Fig. 8j and 8l). The continual decrease in water storage
612 over western basins is likely caused by the interaction of complex climate patterns like El
613 Niño Southern Oscillation, Indian Ocean Dipole, and Southern Annular Mode cycles
614 (Australian Bureau of Meteorology, 2012; Xie et al., 2016).
615

616 **5.5 Comparison of GC approach with alternatives**

617 The simplest approach to estimate ΔGWS is to subtract the model soil moisture component
618 from GRACE ΔTWS data, without considering uncertainty in the model output, as used in
619 Rodell et al. (2009) and Famiglietti et al. (2011). This method is called Approach 1 (App 1).
620 In Approach 2 (App 2) as in Tangdamrongsub et al. (2017), by accounting for the uncertainty

Deleted: 6. Further development of GC approach¶
6.1

623 of model outputs and GRACE data, the water storage states are updated through a Kalman
 624 filter:

$$625 \quad \hat{\mathbf{h}}_R = \tilde{\mathbf{h}}_R + \mathbf{H}\mathbf{C}_R^T(\mathbf{H}\mathbf{R}\mathbf{H}^T + \mathbf{C}_R)^{-1}(\mathbf{b} - \mathbf{H}\tilde{\mathbf{h}}_R) \quad (20)$$

626 where $\tilde{\mathbf{h}}_R$, \mathbf{H} , \mathbf{C}_R are described in Sect. 2, \mathbf{b} is an observation vector containing GRACE-
 627 derived ΔTWS , and \mathbf{R} is an error variance-covariance matrix of the observation. The
 628 GRACE-derived ΔTWS and its error information is obtained from the mascon solution. The
 629 matrix \mathbf{R} is a (diagonal) error variance matrix since no covariance information is given in the
 630 mascon product. Note that the model uncertainty remains the same as in GC approach (Sect.
 631 4.2). The different results from App1 and App2 are mainly attributed to the different estimates
 632 of the uncertainty.

633 The ΔGWS estimates from App1, App2 and GC in Queensland and Victoria are shown in
 634 Fig. 9. It is clearly seen that ΔGWS from App1 are overestimated while the one from App2
 635 fits the ground data significantly better. This behaviour was also seen in Tangdamrongsub et
 636 al. (2017) that the water storage estimates tend to be overestimated when error components
 637 such as spatial correlation error were neglected as in App1. ΔGWS from App2 shows clear
 638 improvements in terms of NS coefficients in both networks. Considering the de-seasonalized
 639 ΔGWS estimates, in Queensland, the trend increases from 0.39 ± 0.03 to 0.42 ± 0.03 cm/year
 640 (improves by 1.5%), and the NS value increases from 0.46 to 0.53. In Victoria, the trend
 641 decreases from 0.73 ± 0.10 to 0.46 ± 0.05 cm/year (improves by 27%), and the NS value
 642 increases from -0.89 to 0.30. Although App2 is not yet as good as the GC solution based on
 643 the most comprehensive error propagation, this simple test demonstrates an important of
 644 considering the uncertainty. The reason of App2 being less accurate than GC is likely due to
 645 too simplified error information implemented in App2.
 646

647 **6. Conclusion**

648 This study presents an approach of combining the raw GRACE observation with model
 649 simulation to improve water storage estimates over Australia. Distinct from other methods,
 650 we exploit the fundamental GRACE satellite tracking data and the full data error variance-
 651 covariance information to avoid alteration of signal and measurement error information
 652 present in higher level data products.

653 We compare groundwater storage estimates from GC approach and two other approaches,
 654 subject to inclusion of GRACE uncertainty in ΔGWS calculation. Validating three results of
 655 ΔGWS against the in situ groundwater data, we find that the GC approach delivers the most
 656 accurate groundwater estimate, followed by the approach based on incomplete information of
 657 GRACE's data error. The poorest estimate of groundwater storage is seen when the GRACE
 658 uncertainty is completely ignored. This confirms the critical value of using the complete
 659 GRACE signal and error information at the raw data level.

660 The analysis of water storage change between 2003 and 2016 reveals that half of the
 661 continent (5 out of 10 basins) is still not fully recovered from the Millennium Drought. The
 662 TWS decrease in Western Australia has been most characteristic and the GC approach finds
 663 that the water loss mainly occur in groundwater layer. Rainfall inadequacy is attributed to the

Deleted: outputs

Deleted: between

Deleted: 6.2 GC data assimilation approach¶

We so far discussed the GC approach to update the water storage estimates independently every month. The approach can be easily expanded to sequentially update the model initial states whenever the GRACE observation is available (for example, every day) as in data assimilation (DA) like ensemble Kalman filter (Evensen, 2003) and particle filter (Weerts and El Serafy, 2006). We briefly describe a way of modifying the GC approach suitable for DA. The ensemble of simulated monthly water storage estimates is predicted based on the set of ensemble forcing data and model parameters. This is simply running CABLE for K (number of ensemble) times. When GRACE observation is available, the updated state is computed: ¶

$$\hat{\mathbf{h}}_{Re} = (\mathbf{C}_R + \mathbf{N}_R)^{-1}(\mathbf{C}_R\tilde{\mathbf{h}}_{Re} + \mathbf{c}_{Re}) \quad (21)¶$$

where the subscript e represents the ensemble or perturbed version of the original vector or matrix (see e.g., Eq. (11)). The dimension of $\tilde{\mathbf{h}}_{Re}$, $\hat{\mathbf{h}}_{Re}$, \mathbf{c}_{Re} is $3 \times K$. The estimated $\hat{\mathbf{h}}_{Re}$ can be directly used as in the initial state for the next time step for CABLE run (Eicker et al., 2014; Tangdamrongsub et al., 2015; Tian et al., 2017), or used in the repeated run to avoid any spurious jump of the water storage estimates between the each step (Forman et al., 2012; Tangdamrongsub et al., 2017). This sequential update process can be carried out as long as desired. The feasibility of GRACE DA has been demonstrated with "devised" uncertainty (covariance) information. As a future work, we will develop new DA approach on the basis of full error information of GRACE data by using the least-squares normal equation and thus carrying the error information from the fundamental (satellite tracking) data level. ¶

7

696 continual dry condition, leading to a greater decreasing of groundwater recharge and storage
697 over Western Australia.

698 The land surface model we used is deficient in anthropogenic groundwater consumption. The
699 model calibration will never help and the groundwater consumption must be brought in by
700 external sources. On the contrary, the statistical approach like our GC approach may be
701 useful to fill in the missing component and lead to a more comprehensive water storage
702 inventory.

703 However, it is difficult to constrain different water storage components by only using total
704 storage observation like GRACE. In addition, it is challenging to improve surface soil
705 moisture varying rapidly in time, using a monthly mean GRACE observation. Tian et al.
706 (2017) utilized the satellite soil moisture observation from the Soil Moisture and Ocean
707 Salinity (SMOS, Kerr et al., 2001) in addition to GRACE data for their data assimilation and
708 showed a clear improvement in the top soil moisture estimate. The GC approach with
709 complementary observations at higher temporal resolution should be considered particularly
710 to enhance the surface soil moisture computation.

711 Finally, the GC approach can be simply extended for GRACE data assimilation. Assimilating
712 the raw GRACE data into land surface models like CABLE enables the model state and
713 parameter to be adjusted with the realistic error information, allowing reliable storage
714 computation. The GC data assimilation will be developed in our future study.

715

716 Acknowledgement

717 This work was funded by NASA projects on GRACE and GRACE Follow-On missions and
718 partly by Australian Research Council (DP160104095). MD was supported by ARC Centre
719 of Excellence for Climate Systems Science. HK was supported by Japan Society for the
720 Promotion of Science KAKENHI (16H06291). We thank Torsten Mayer-Gürr for GRACE
721 data products in the form of the least-squares normal equations. We also thank three
722 anonymous reviewers for helping us improve the manuscript.

723

- Deleted: is
- Deleted: University of Newcastle to support
- Deleted: 's
- Deleted: .
- Deleted: ark
- Deleted: ecker
- Deleted: yungjun
- Deleted: im
- Deleted:

733 **Appendix: Nash-Sutcliff coefficient and area-weighted average**

734 Nash-Sutcliff coefficient (NS) is computed as follows:

735
$$NS = 1 - \frac{\sum_{i=1}^N (\mathbf{y}_i - \hat{\mathbf{x}}_i)^2}{\sum_{i=1}^N (\mathbf{y}_i - \bar{\mathbf{y}})^2} \quad (A1)$$

736 where \mathbf{y} is an observation vector, $\bar{\mathbf{y}}$ is the mean of the observation, $\hat{\mathbf{x}}$ is a vector containing
737 the simulated result, i is the index of observation, and N is the number of observation.

738 Area-weighted average (\bar{Z}) is compute as follows:

739
$$\bar{Z} = \frac{\sum_{j=1}^M w_j \bar{z}_j}{\sum_{j=1}^M w_j} \quad (A2)$$

740 where w is the area size, \bar{z} is the mean value inside the considered area, j is the area index,
741 and M is the number of considered area.

742

743 **References**

- 744 Australian Bureau of Meteorology (2012) Record-breaking La Niña events: An analysis of
745 the La Niña life cycle and the impacts and significance of the 2010–11 and 2011–12 La Niña
746 events in Australia, National Climate Centre, Bureau of Meteorology,
747 <http://www.bom.gov.au/climate/enso/history/La-Nina-2010-12.pdf> (last accessed: 5 January
748 2017).
- 749 Bettadpur, S.: CSR Level-2 Processing Standards Document for Product Release 05, GRACE
750 327-742, Center for Space Research, The University of Texas at Austin, 2012.
- 751 Chen, J. L., Wilson, C. R., Tapley, B. D., Scanlon, B., Güntner, A.: Long-term groundwater
752 storage change in Victoria, Australia from satellite gravity and in situ observations, *Glob.*
753 *Planet. Change*, 139, 56–65, doi: <http://dx.doi.org/10.1016/j.gloplacha.2016.01.002>, 2016.
- 754 Decker, M.: Development and evaluation of a new soil moisture and runoff parameterization
755 for the CABLE LSM including subgrid-scale processes, *J. Adv. Model. Earth Syst.*, 7, 1788–
756 1809, doi:10.1002/2015MS000507, 2015.
- 757 Dee, D. P., Uppala, S. M., Simmons, A. J., Berrisford, P., Poli, P., Kobayashi, S., Andrae, U.,
758 Balmaseda, M. A., Balsamo, G., Bauer, P., Bechtold, P., Beljaars, A. C. M., van de Berg, L.,
759 Bidlot, J., Bormann, N., Delsol, C., Dragani, R., Fuentes, M., Geer, A. J., Haiberger, L.,
760 Healy, S. B., Hersbach, H., Hólm, E. V., Isaksen, L., Kállberg, P., Köhler, M., Matricardi,
761 M., McNally, A. P., Monge-Sanz, B. M., Morcrette, J. J., Park, B. K., Peubey, C., de Rosnay,
762 P., Tavolato, C., Thépaut, J. N., and Vitart, F.: The ERA-Interim reanalysis: configuration
763 and performance of the data assimilation system. *Quarterly Journal of the Royal*
764 *Meteorological Society*, 137, 553–597, doi:10.1002/qj.828, 2011.
- 765 Dumedah, G., and Walker, J. P.: Intercomparison of the JULES and CALBE land surface
766 models through assimilation of remote sensed soil moisture in southeast Australia, *Adv. Wat.*
767 *Res.*, 74, 231 – 244, doi:[hmap://dx.doi.org/10.1016/j.advwatres.2014.09.011](http://dx.doi.org/10.1016/j.advwatres.2014.09.011), 2014.
- 768 Eicker, A., Schumacher, M., Kusche, J., Döll, P., and Müller Schmied, H.: Calibration data
769 assimilation approach for integrating GRACE data into the WaterGAP Global Hydrology
770 Model (WGHM) using an Ensemble Kalman Filter: First Results, *Surv. Geophys.*, 35(6),
771 1285-1309, doi:10.1007/s10712-014-9309-8, 2014.
- 772 Evensen, G.: The ensemble Kalman filter: Theoretical formulation and practical
773 implementation, *Ocean Dyn.*, 53(4), 343-367, doi:10.1007/S10236-003-0036-9, 2003.
- 774 Famiglietti, J. S., Lo, M., Ho, S. L., Bethune, J., Anderson, K. J., Syed, T. H., Swenson, S.
775 C., de Linage, C. R., and Rodell, M.: Satellites measure recent rates of groundwater depletion
776 in California’s Central Valley, *Geophys. Res. Lett.*, 38, L03403, doi:10.1029/2010GL046442,
777 2011.
- 778 Fasullo, J. T., Boening, C., Landerer, F. W., and Nerem, R. S.: Australia’s unique influence
779 on global sea level in 2010–2011, *Geophys. Res. Lett.*, 40, 4368–4373,
780 doi:10.1002/grl.50834, 2013.
- 781 Forman, B. A., Reichle, R. H., and Rodell, M.: Assimilation of terrestrial water storage from
782 GRACE in a snow-dominated basin, *Water Resour. Res.*, 48, W01507,
783 doi:10.1029/2011WR011239, 2012.

Deleted: Dirmeyer, P. A.: A history and review of the Global Soil Wetness Project (GSWP), *J. Hydrometeorol.*, 12, 729–749, doi:10.1175/JHM-D-10-05010.1, 2011.¶

787 [Forootan, E., Safari, A., Mostafaie, A., Schumacher, M., Delavar, M., and Awange, J. L.:](#)
788 [Large-Scale Total Water Storage and Water Flux Changes over the Arid and Semiarid Parts](#)
789 [of the Middle East from GRACE and Reanalysis Products, *Surv. Geophys.*, 38:591-615,](#)
790 [doi:10.1007/s10712-016-9403-1, 2017.](#)

791 Giroto, M., De Lannoy, G. J. M., Reichle, R. H., and Rodell, M.: Assimilation of gridded
792 terrestrial water storage observations from GRACE into a land surface model, *Water Resour.*
793 *Res.*, 52(5), 4164–4183, doi:10.1002/2015WR018417, 2016.

794 Hamill, T. M., Whitaker, J. S., and Snyder, C.: Distance-Dependent Filtering of Background
795 Error Covariance Estimates in an Ensemble Kalman Filter, *Mon. Weather Rev.*, 129, 2776–
796 2790, 2001.

797 Han, S.-C.: Elastic deformation of the Australian continent induced by seasonal water cycles
798 and the 2010-11 La Niña determined using GPS and GRACE, *Geophys. Res. Lett.*, 44, doi:
799 10.1002/2017GL072999, 2017.

800 Huffman, G. J., Adler, R. F., Bolvin, D. T., Gu, G., Nelkin, E. J., Bowman, K. P., Hong, Y.,
801 Stocker, E. F., and Wolf, D. B.: The TRMM multisatellite precipitation analysis (TMPA):
802 Quasi-global, multiyear, combined-sensor precipitation estimates at fine scales, *J.*
803 *Hydrometeor.*, 8, 38–55, doi:10.1175/JHM560.1, 2007.

804 Jekeli, C.: Alternative methods to smooth the Earth’s gravity field, Rep., 327, Dept. of Geod.
805 Sci. and Surv., Ohio State Univ., Columbus, 1981.

806 Kerr, Y. H., Waldteufel, P., Wigneron, J.-P., Martinuzzi, J.-M., Font, J., and Berger, M.: Soil
807 moisture retrieval from space: The soil moisture and ocean salinity (SMOS) mission, *IEEE*
808 *Trans. Geosci. Remote Sens.*, 39(8), 1729–1735, 2001.

809 Lambert, A., Huang, J., van der Kamp, G., Henton, J., Mazzotti, S., James, T. S., Courtier,
810 N., and Barr, A. G.: Measuring water accumulation rates using GRACE data in areas
811 experiencing glacial isostatic adjustment: The Nelson River basin, *Geophys. Res. Lett.*, 40,
812 6118–6122, doi:10.1002/2013GL057973, 2013.

813 Landerer, F. W., and Swenson, S. C.: Accuracy of scaled GRACE terrestrial water storage
814 estimates, *Water Resour. Res.*, 48, W04531, doi:10.1029/2011WR011453, 2012.

815 Leblanc, M., Tweed, S., Van Dijk, A., Timbal, B.: A review of historic and future
816 hydrological changes in the Murray-Darling Basin, *Global and Planetary Change*, 80 – 81,
817 226 – 246, doi:10.1016/j.gloplacha.2011.10.012, 2012.

818 Lemoine, J. M., Bourgoigne, S., Bruinsma, S., Gégout, P., Reinquin, F., Biancale R.: GRACE
819 RL03-v2 monthly time series of solutions from CNES/GRGS, EGU2015-14461, EGU
820 General Assembly 2015, Vienna, Austria, 2015.

821 Mayer-Gürr, T., Behzadpour, S., Ellmer, M., Kvas, A., Klinger, B., Zehentner, N.: ITSG-
822 Grace2016 - Monthly and Daily Gravity Field Solutions from GRACE. GFZ Data Services.
823 <http://doi.org/10.5880/icgem.2016.007>, 2016.

824 Mayer-Gürr T., Pail R., Gruber T., Fecher T., Rexer M., Schuh W.-D., Kusche J., Brockmann
825 J.-M., Rieser D., Zehentner N., Kvas A., Klinger B., Baur O., Höck E., Krauss S., Jäggi A.:
826 The combined satellite gravity field model GOCO05s, EGU 2015, Vienna, 2015.

827 McGrath, G. S., Sadler, R., Fleming, K., Tregoning, P., Hinz, C., and Veneklaas, E. J.:
828 Tropical cyclones and the ecohydrology of Australia's recent continental-scale drought,
829 *Geophys. Res. Lett.*, 39, L03404, doi:10.1029/2011GL050263, 2012.

830 Njoku, E. G., Jackson, T. L., Lakshmi, V., Chan, T., Nghiem, S. V.: Soil Moisture Retrieval
831 from AMSR-E, *IEEE T. Geosci. Remote*, 41 (2): 215-229, 2003.

832 Owe, M., de Jeu, R., Holmes, T.: Multisensor historical climatology of satellite-derived global
833 land surface moisture, *J. Geophys. Res.*, 113, F01002, 17 pp., doi:10.1029/2007JF000769,
834 2008.

835 Pearson, E. K.: Mining imperfect data: Dealing with contamination and incomplete records,
836 ProSanos Corporation, Harrisburg, Pennsylvania, ISBN: 978-0-89871-582-8, doi:
837 <http://dx.doi.org/10.1137/1.9780898717884>, 2005.

838 Rassam, D. W., Peeters, L., Pickett, T., Jolly, I., Holz, L.: Accounting for
839 surface-groundwater interactions and their uncertainty in river and groundwater models: A
840 case study in the Namoi River, Australia, *Environ. Modell. Softw.*, 50, 108-119,
841 <http://dx.doi.org/10.1016/j.envsoft.2013.09.004>, 2013.

842 Reichle, R. H., and Koster, R. D.: Bias reduction in short records of satellite soil moisture,
843 *Geophys. Res. Lett.*, 31, L19501, doi:10.1029/2004GL020938, 2004.

844 Rienecker, M. M., Suarez, M. J., Gelaro R, Todling R, Bacmeister J, Liu E, Bosilovich MG,
845 Schubert SD, Takacs L, Kim G-K, Bloom S, Chen J, Collins D, Conaty A, da Silva A, Gu W,
846 Joiner J, Koster RD, Lucchesi R, Molod A, Owens T, Pawson S, Pegion P, Redder CR,
847 Reichle R, Robertson FR, Ruddick AG, Sienkiewicz M, Woollen J. 2011. MERRA—NASA's
848 Modern-Era Retrospective Analysis for Research and Applications. *J. Climate*, DOI:
849 10.1175/JCLI-D-11-00015.1.

850 [Rietbroek, R., Fritsche, M., Brunnabend, S.-E., Daras, I., Kusche, J., Schröter, J., Flechtner,](#)
851 [F., and Dietrich, R.: Global surface mass from a new combination of GRACE, modelled OBP](#)
852 [and reprocessed GPS data, *J. Geodyn.*, 59 - 60:64 - 71, doi:10.1016/j.jog.2011.02.003, 2012.](#)

853 Rodell, M., Houser, P. R., Jambor, U., Gottschalck, J., Mitchell, K., Meng, C. J., Arsenault,
854 K., Cosgrove, B., Radakovich, J., Bosilovich, M., Entin, J. K., Walker, J. P., Lohmann, D.,
855 and Toll, D.: The global land data assimilation system, *Bull. Amer. Meteor. Soc.*, 85(3), 381–
856 394, 2004.

857 Rodell, M., Velicogna, I., Famiglietti, J. S.: Satellite-based estimates of groundwater
858 depletion in India, *Nature*. 460, 999-1002, doi:10.1038/nature08238, 2009.

859 Sakumura, C., Bettadpur, S., and Bruinsma, S.: Ensemble prediction and intercomparison
860 analysis of GRACE time-variable gravity field models, *Geophys. Res. Lett.*, 41, 1389–1397,
861 doi:10.1002/2013GL058632, 2014.

862 [Schmeer, M., Schmidt, M., Boschb, W., and Seitz, F.: Separation of mass signals within](#)
863 [GRACE monthly gravity field models by means of empirical orthogonal functions, *J.*](#)
864 [Geodyn.](#), 59 - 60:124 - 132, doi:10.1016/j.jog.2012.03.001, 2012.

865 Sheffield, J., Goteti, G., and Wood, E. F.: Development of a 50-yr high-resolution global
866 dataset of meteorological forcings for land surface modeling, *J. Climate*, 19 (13), 3088-3111,
867 2005.

868 Schumacher, M., Kusche, J., and Döll, P.: A Systematic Impact Assessment of GRACE Error
869 Correlation on Data Assimilation in Hydrological Models, *J. Geod.*, 90(6), 537–559.
870 doi:10.1007/s00190-016-0892-y, 2016.

871 Sorooshian, S., Hsu, K., Gao, X., Gupta, H. V., Imam, B., and Braithwaite, D.: Evaluation of
872 PERSIANN System Satellite-Based Estimates of Tropical Rainfall, *Bulletin of the American
873 Meteorological Society*, Vol. 81, No. 9, 2035-2046, 2000.

874 Swenson, S. C.: GRACE monthly land water mass grids NETCDF RELEASE 5.0. Ver. 5.0.
875 PO.DAAC, CA, USA, <http://dx.doi.org/10.5067/TELND-NC005>, 2012. (last accessed: 5
876 January 2017).

877 Swenson, S. and Wahr, J.: Post-processing removal of correlated errors in GRACE data,
878 *Geophys. Res. Lett.*, 33(L08402), doi:10.1029/2005GL025285, 2006.

879 Tangdamrongsub, N., Ditmar, P. G., Steele-Dunne, S. C., Gunter, B. C., Sutanudjaja, E. H.
880 (2016) Assessing total water storage and identifying flood events over Tonlé Sap basin in
881 Cambodia using GRACE and MODIS satellite observations combined with hydrological
882 models, *Remote Sens. Environ.*, 181, 162–173,
883 doi:<http://dx.doi.org/10.1016/j.rse.2016.03.030>.

884 Tangdamrongsub, N., Steele-Dunne, S. C., Gunter, B. C., Ditmar, P. G., and Weerts, A. H.:
885 Data assimilation of GRACE terrestrial water storage estimates into a regional hydrological
886 model of the Rhine River basin, *Hydrol. Earth Syst. Sci.*, 19, 2079–2100, doi:10.5194/hess-
887 19-2079-2015, 2015.

888 Tangdamrongsub, N., Steele-Dunne, S. C., Gunter, B. C., Ditmar, P. G., Sutanudjaja, E. H.,
889 Xie, T, Wang, Z.: Improving estimates of water resources in a semi-arid region by
890 assimilating GRACE data into the PCR-GLOBWB hydrological model, *Hydrol. Earth Syst.
891 Sci.*, 21, 2053 – 2074, doi:10.5194/hess-21-2053-2017, 2017.

892 Tian, S., Tregoning, P., Renzullo, L. J., van Dijk, A. I. J. M., Walker, J. P., Pauwels, V. R. N.,
893 Allgeyer, S.: Improved water balance component estimates through joint assimilation of
894 GRACE water storage and SMOS soil moisture retrievals, *Water Resour. Res.*, 53,
895 doi:10.1002/2016WR019641, 2017.

896 Trenberth, K. E.: Framing the way to relate climate extremes to climate change, *Climatic
897 Change*, 115 283–290 , doi:10.1007/s10584-012-0441-5, 2012.

898 Tscherning, C. C. and Rapp R. H.: Closed covariance expressions for gravity anomalies,
899 geoid undulations, and deflections of the vertical implied by anomaly degree variance
900 models, Rep. 208, Dep. of Geod. Sci. and Surv., Ohio State Univ., Columbus, 1974.

901 Ukkola, A. M., Pitman, A. J., Decker, M., De Kauwe, M. G., Abramowitz, G., Kala, J., and
902 Wang, Y.-P.: Modelling evapotranspiration during precipitation deficits: identifying critical
903 processes in a land surface model. *Hydrol. Earth Syst. Sci.*, 20, 2403–2419, doi:10.5194/hess-
904 20-2403-2016, 2016.

905 Van Dijk, A., Beck, H. E., Crosbie, R. S., De Jeu, E. A. M., Liu, Y. Y., Podger, G. M.,
906 Timbal, B., Viney, N. R.: The Millennium Drought in southeast Australia (2001–2009):
907 Natural and human causes and implications for water resources, ecosystems, economy, and
908 society, *Water Resour. Res.*, 49 (2), 1040 - 1057, doi:10.1002/wrcr.20123, 2013.

909 Van Dijk, A., Podger, G., Kirby, M.: Integrated water resources management in the Murray-
910 Darling Basin. In: Schumann, A., Pahlow, M. (Eds.), *Increasing demands on decreasing
911 supplies, in Reducing the Vulnerability of Societies to Water Related Risks at the Basin
912 Scale*, IAHS Publ. 24–30, 2007.

913 Voss, K. A., Famiglietti, J. S., Lo, M., de Linage, C., Rodell, M., and Swenson, S. C.:
914 Groundwater depletion in the Middle East from GRACE with implications for transboundary
915 water management in the Tigris-Euphrates-Western Iran region, *Water Resour. Res.*, 49,
916 doi:10.1002/wrcr.20078, 2013.

917 Wahr, J., Molenaar, M., and Bryan, F.: Time variability of the Earth's gravity field:
918 Hydrological and oceanic effects and their possible detection using GRACE, *J. Geophys.
919 Res.*, 103(B12), 30205–30229, 1998.

920 Wahr, J., Swenson, S., and Velicogna, I.: Accuracy of GRACE mass estimates, *Geophys.
921 Res. Lett.*, 33, L06401, doi:10.1029/2005GL025305, 2006.

922 Watkins, M. M., Wiese, D. N., Yuan, D.-N., Boening, C., and Landerer, F. W.: Improved
923 methods for observing Earth's time variable mass distribution with GRACE using spherical
924 cap mascons, *J. Geophys. Res. Solid Earth*, 120, 2648–2671, doi:10.1002/2014JB011547,
925 2015.

926 Weerts, A. H. and El Serafy G. Y. H.: Particle filtering and ensemble Kalman filtering for
927 state updating with hydrological conceptual rainfall-runoff models, *Water Resour. Res.*, 42,
928 W09403, doi:10.1029/2005WR004093, 2006.

929 Welsh, W.D.: Water balance modelling in Bowen, Queensland, and the ten iterative steps in
930 model development and evaluation, *Environ. Modell. Softw.*, 23 (2), 195-205, 2008.

931 Wiese, D. N., Landerer, F. W., and Watkins, M. M.: Quantifying and reducing leakage errors
932 in the JPL RL05M GRACE mascon solution, *Water Resour. Res.*, 52, 7490–7502,
933 doi:10.1002/2016WR019344, 2016.

934 Wu, S. C., Kruizinga, G., and Bertiger, W.: Algorithm theoretical basis document for
935 GRACE Level-1B data processing V1.2, JPL D-27672, Jet Propul. Lab., Pasadena, Calif,
936 2006.

937 Xie, Z., Huete, A., Restrepo-Coupea, N., Maa, X., Devadasa, R., Caprarellob, G.: Spatial
938 partitioning and temporal evolution of Australia's total water storage under extreme
939 hydroclimatic impacts, *Remote Sens. Environ.*, 183, 43–52,
940 <http://dx.doi.org/10.1016/j.rse.2016.05.017>, 2016.

941 Zaitchik, B. F., Rodell, M., and Reichle, E. H.: Assimilation of GRACE terrestrial water
942 storage data into a land surface model: Results for the Mississippi basin, *Amer. Meteor. Soc.*,
943 *J. Hydrometeor.*, 9, 535–548, 2008.

944

945 **Table 1.** Precipitation data from 7 different products used in this study, the Global Soil
946 Wetness Project Phase 3 (GSWP3), the Global Land Data Assimilation System (GLDAS),
947 the Tropical Rainfall Measuring Mission (TRMM), the Modern-Era Retrospective Analysis
948 for Research and Applications (MERRA), the European Centre for Medium-Range Weather
949 Forecasts (ECMWF), the Princeton's Global Meteorological Forcing Dataset (Princeton), and
950 the Precipitation Estimation from Remotely Sensed Information using Artificial Neural
951 Networks (PERSIANN). The temporal resolution of all products are 3 hours. Most products
952 are available to present while GSWP3, MERRA, and Princeton terminate earlier.

Product	Availability	Spatial resolution	References
GSWP3	1901/01 – 2010/12	0.5°×0.5°	http://hydro.iis.u-tokyo.ac.jp/GSWP3
GLDAS (NOAH025SUBP 3H)	2000/03 – present	0.25°×0.25°	Rodell et al. (2004)
TRMM (3B42)	1998/01 – present	0.25°×0.25°	Huffman et al. (2007)
MERRA (MSTMNXMLD.5.2.0)	1980/01 – 2016/02	0.5°×0.67°	Rienecker et al. (2011)
ECMWF (ERA-Interim)	1979/01 – present	0.75°×0.75°	Dee et al. (2011)
Princeton (V2 0.5°)	1987/01 – 2012/12	0.5°×0.5°	Sheffield et al. (2005)
PERSIANN (3 hr)	2002/03 – present	0.25°×0.25°	Sorooshian et al. (2000)

953

954

955 **Table 2.** Model parameters that are sensitive to SM and GWS estimates. The following
956 parameters were perturbed using the additive noise with the boundary conditions given in the
957 last column. The further parameter description can be found in Decker (2015) and Ukkola et
958 al. (2016).

Parameter	Name	Spatial variability	Perturbed range
$f_{\text{clay}}, f_{\text{sand}}, f_{\text{silt}}$	Fraction of clay, sand, and silt	Yes	0 – 1
f_{sat}	Fraction of grid cell that is saturated	No	810 – 990
q_{sub}	Maximum rate of subsurface drainage assuming a fully saturated soil column	No	0.009 – 0.01
f_{p}	Tuneable parameter controlling drainage speed	No	1.9 – 2.2

959

960

961 **Table 3.** NS coefficients between top soil moisture estimates and the satellite soil moisture
 962 observations from AMSR-E products over 10 different Australian basins. The area-weighted
 963 average value (AVG) is also shown.

	C-band		X-band	
	CABLE	GC	CABLE	GC
GOC	0.67	0.68	0.58	0.60
IND	0.53	0.54	0.41	0.41
LKE	0.48	0.53	0.36	0.42
MRD	0.77	0.80	0.75	0.78
NEC	0.34	0.39	0.14	0.19
NWP	0.33	0.36	0.38	0.42
SEC	0.68	0.68	0.69	0.71
SWC	0.85	0.85	0.89	0.89
SWP	0.55	0.56	0.46	0.48
TIM	0.44	0.45	0.16	0.16
AVG	0.53	0.56	0.47	0.50

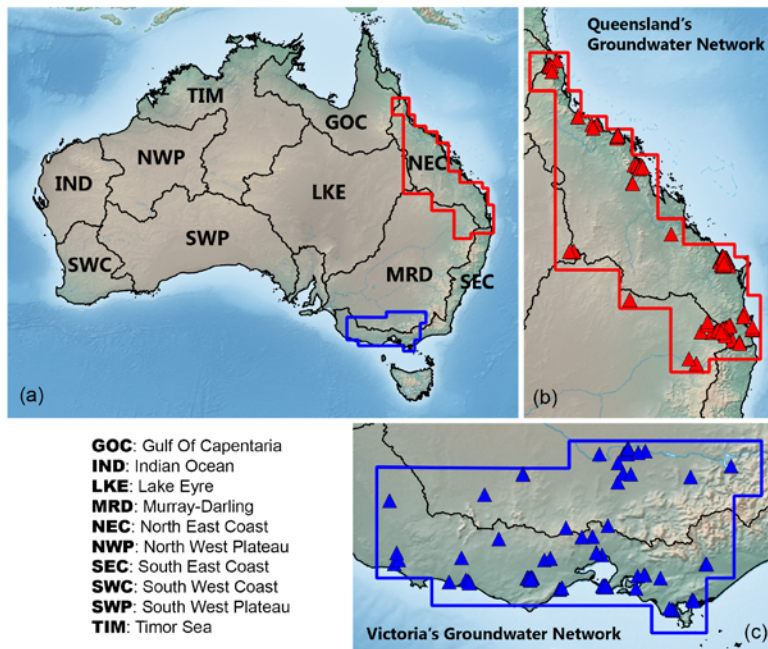
964

965

966 **Table 4.** NS coefficient and long-term trend of ΔGWS estimated from the model-only and
 967 GC solutions in Queensland and Victoria groundwater network. The long-term trend of the
 968 in-situ data is also shown.

	Queensland			Victoria		
	In-situ	CABLE	GC	In-situ	CABLE	GC
Original time-series						
NS [-]	-	0.49	0.60	-	0.34	0.63
Trend [cm/year]	1.60 ± 0.05	0.39 ± 0.02	0.63 ± 0.05	-0.27 ± 0.05	0.10 ± 0.02	-0.18 ± 0.03
De-seasonalized time-series						
NS [-]	-	0.50	0.66	-	0.43	0.83
Trend [cm/year]	1.60 ± 0.05	0.39 ± 0.02	0.57 ± 0.04	-0.25 ± 0.05	0.10 ± 0.02	-0.16 ± 0.03

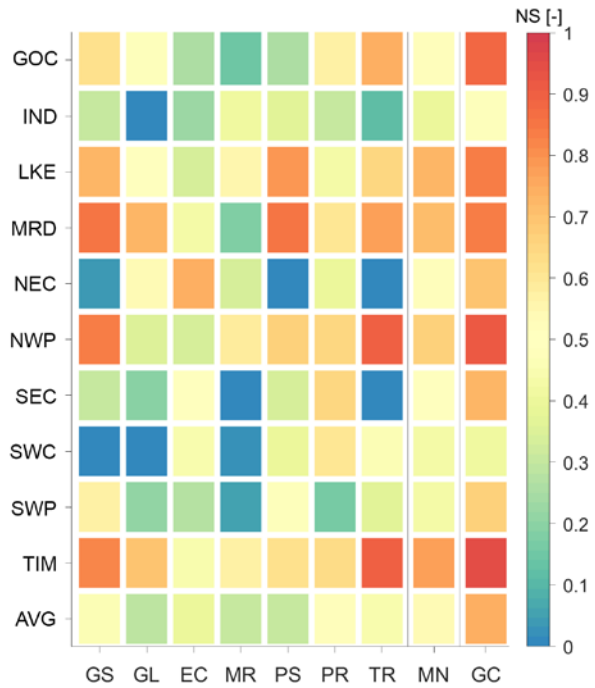
969



970

971 **Figure 1.** (a) Geographical location of 10 Australian river basins. Red and blue polygons
 972 indicate the boundaries of groundwater networks in Queensland (b) and Victoria (c),
 973 respectively. Triangles (in b and c) represent the selected bore locations used in this study.

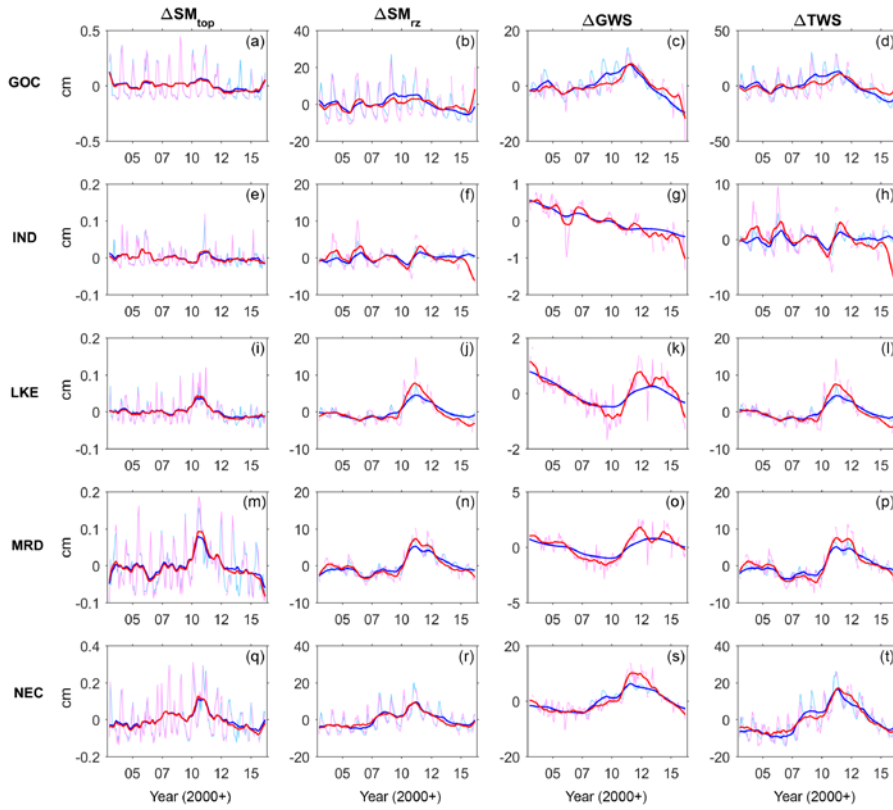
974



975

976 **Figure 2.** NS coefficients between the model and GRACE-mascon ΔTWS over 10 Australian
 977 basins (in ordinate). The NS values were computed based on CABLE ΔTWS computed with
 978 7 different precipitation data (in abscissa), GSWP3 (GS), GLDAS (GL), ECMWF (EC),
 979 MERRA (MR), PERSIANN (PR), TRMM (TR). The NS value of the mean ΔTWS estimates
 980 (the average of 7 variants) is also shown (MN). The area-weighted average NS value over all
 981 basins is also shown (AVG). The NS value of ΔTWS from the GRACE-combined (GC)
 982 approach is shown in the last column. The full name of the basins can be found in Fig. 1.

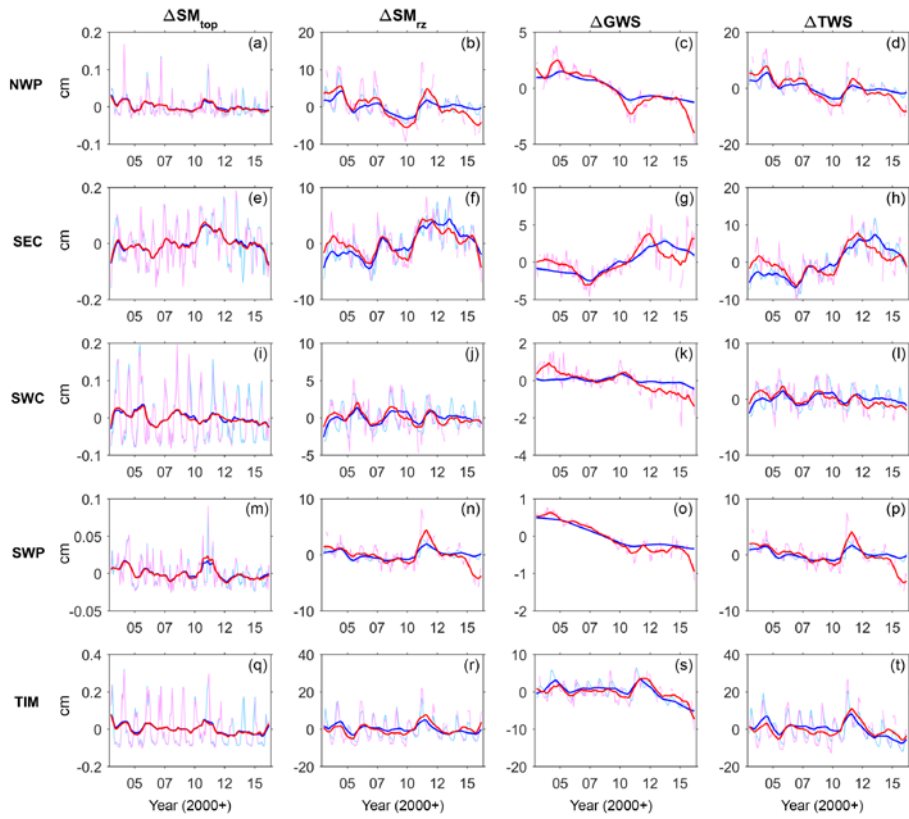
983



984

985 **Figure 3.** The monthly time series of ΔSM_{top} , ΔSM_{rz} , ΔGWS , and ΔTWS estimated from
 986 model (blue) and GC (red) solutions over Gulf of Carpentaria (GOC), Indian Ocean (IND),
 987 Lake Eyre (LKE), Murray-Darling (MRD), and North East Coast (NEC). The de-
 988 seasonalized time series is also shown.

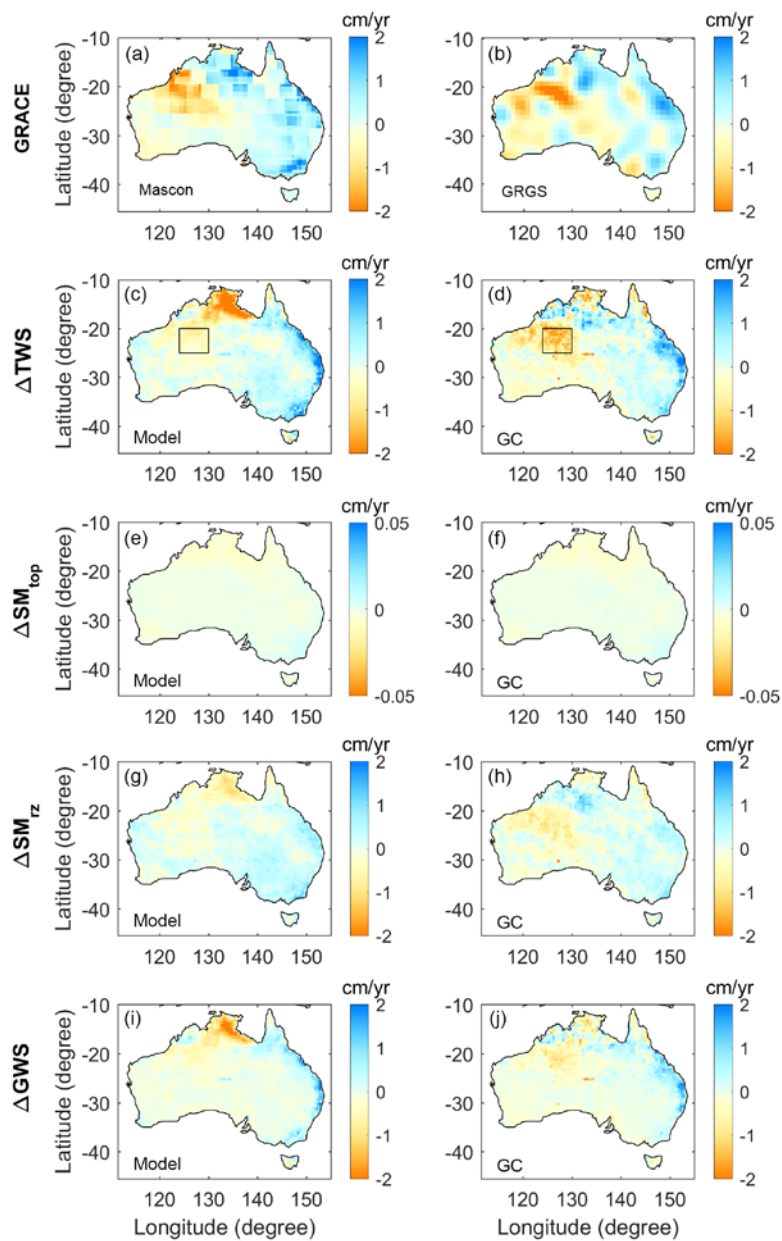
989



990

991 **Figure 4.** Similar to Fig. 3, but estimated over North West Plateau (NWP), South East Coast
 992 (SEC), South West Coast (SWC), South West Plateau (SWP), and Timor Sea (TIM).

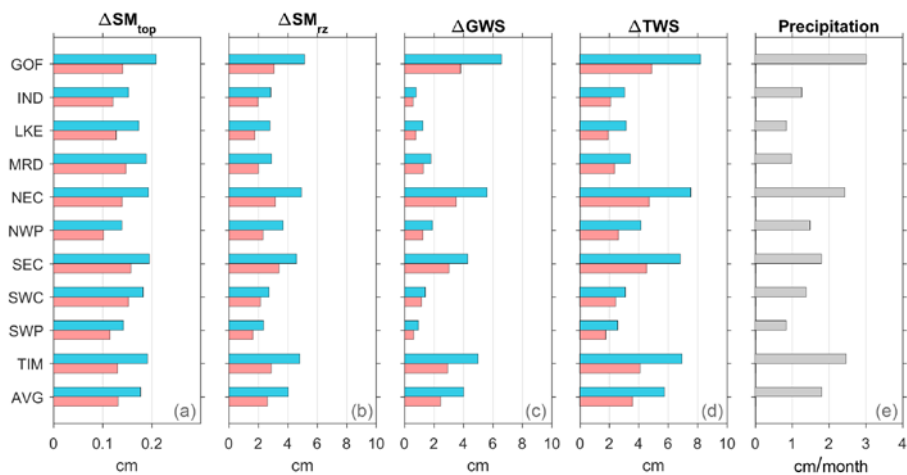
993



994

995 **Figure 5.** Long-term trends of ΔTWS (c, d), ΔSM_{top} (e, f), ΔSM_{rz} (g, h), and ΔGWS (i, j)
 996 estimated from the model-only (left) and the GC solutions (right). Results of GRACE ΔTWS
 997 independently from mascon (a) and GRGS solution (b) are also shown. The eastern part of
 998 North West Plateau basin is shown as a rectangle polygon in (c) and (d).

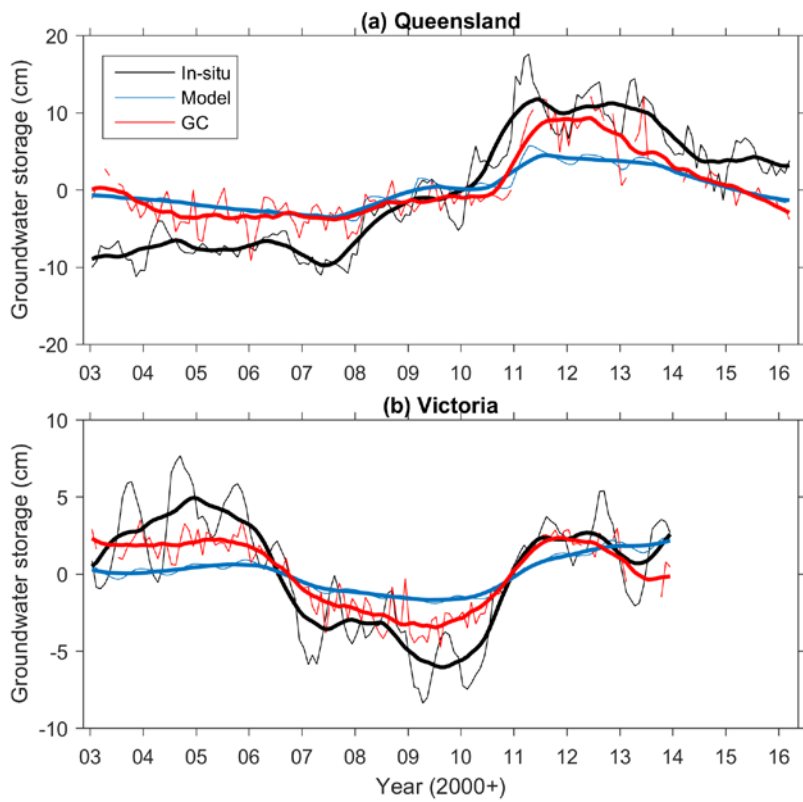
999



1000

1001 **Figure 6.** Uncertainties of ΔSM_{top} , ΔSM_{rz} , ΔGWS , and ΔTWS estimated from the model
 1002 (blue) and the GC solutions (red) in 10 different Australian basins. The uncertainty of the
 1003 precipitation is shown in (e). The area-weighted average value (AVG) is also shown.

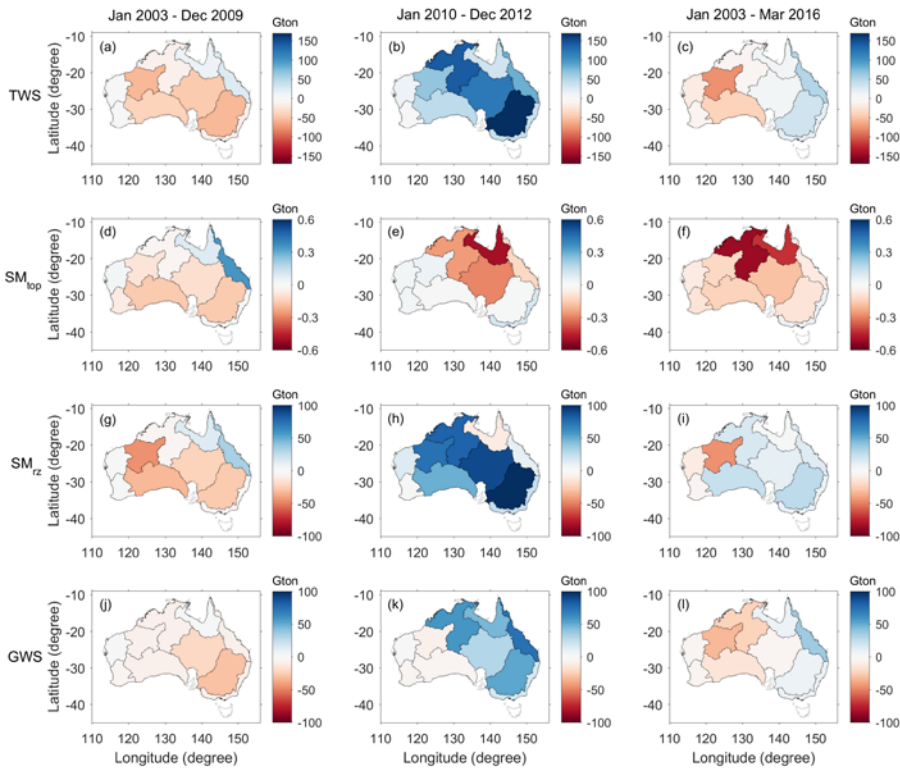
1004



1005

1006 **Figure 7.** The monthly time series of ΔGWS estimated from the model, GC solutions, and
 1007 measured from the in situ groundwater network in Queensland (a) and Victoria (b). De-
 1008 seasonalized time series are shown in thick lines.

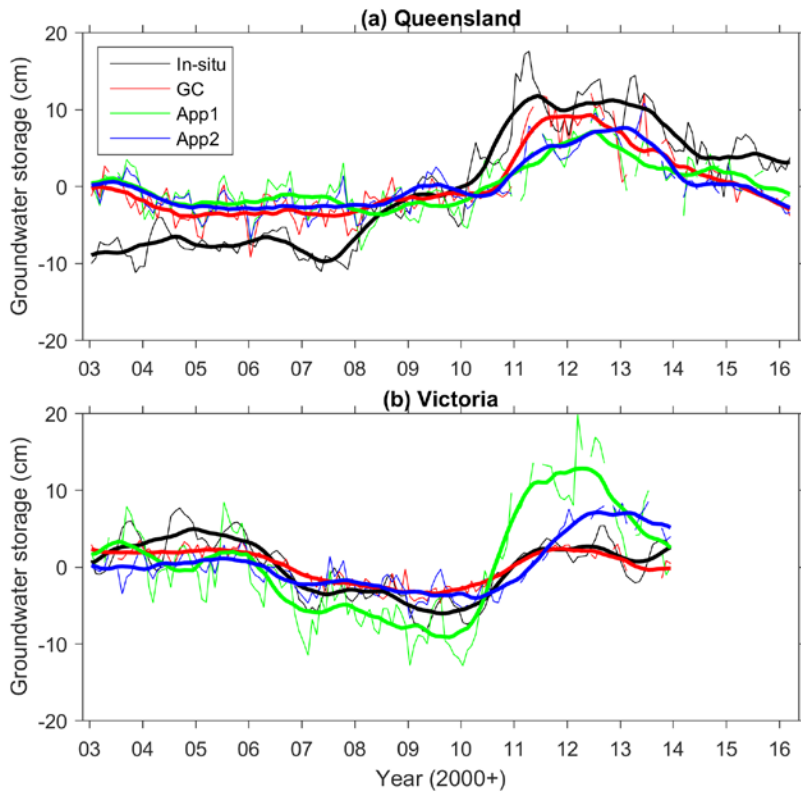
1009



1010

1011 **Figure 8.** Mass changes (Gton, Giga tonne) of ΔTWS , ΔSM_{top} , ΔSM_{rz} , and ΔGWS estimated
 1012 from GC solutions over 10 Australian basins in 3 different periods, Big Dry (January 2003 –
 1013 December 2009), Big Wet (January 2010 – December 2012), and entire period (January 2003
 1014 – March 2016).

1015



1016

1017 **Figure 9.** ΔGWS estimated from Approach 1 (App1) and Approach 2 (App2) in Queensland
 1018 (a) and Victoria (b). The in-situ groundwater network data and the GC solutions are also
 1019 shown. De-seasonalized time series are shown in thick lines.